$\omega(782)$ Reconstruction using photon conversions in pp collisions at $\sqrt{s} = 7$ TeV at the ALICE Experiment

This Bachelor Thesis has been carried out by Carolina Sergi Lopes at the

Institut für Kernphysik at the University of Münster

under the supervision of

Prof. Dr. Johannes Wessels and Priv. Doz. Dr. Christian Klein-Bösing

For Marcelo Barão and Gilmar Mignaco.

ω(782) Reconstruction using photon conversions in pp collisions at $\sqrt{s} = 7$ TeV at the ALICE Experiment

This thesis will analyse the omega particle decay in three pions using the Large Hadron Collider (LHC) data at the ALICE Experiment, taken in 2010 with a center-of-mass energy of 7 TeV. The omega reconstruction is in the beginning performed using photon conversions, which considers decay photon conversions into e^-e^+ pairs and uses this fact to detect γ particles and consequently the neutral pion. Invariant mass plots will be used for the omega signal extractions. The Event Mixing technique will be employed to describe the background and all possible combinatorial background sources will be considered. Monte Carlo simulations will be realized for comparisons with data and also for the omega yield correction. This correction will enable the ω/π^0 ratio measurement.

Contents

List of Figures

List of Tables

1 Physics Overview

This section will give a general overview of the theory used for the omega analysis.

1.1 The Standard Model of Particles

All the experiments and theories since the last century lead physicists to divide the physical interactions of nature in four types of interactions, responsible for ruling the behaviour of particles:

- The gravitational force
- The electromagnetism
- The weak interaction
- The strong interaction

Each force mentioned above has a specific acting range and strength. The weak and the strong interaction have a small acting range, while the electromagnetic and the gravitational force have an infinite one. The weak interaction is, despite its name, stronger than the gravitational force.

Those four interactions happen as if all the particles communicate through force carriers, each one of them having a characteristic carrier [1]. The gravitational force is negligible at subatomic scales and therefore difficult to be investigated. Its supposed force carrier, the graviton, couldn't be proved yet. That's why the scientists couldn't insert the gravity in the so called Standard Model until now.

The Standard Model is a theory based on the three other interactions and affirms the existence of fundamental particles without any internal structure. Those elementary particles are, in this theory, responsible for building heavier particles, as the proton for example. This mentioned elementary constituents of matter can be classified in two different classes: the quarks and leptons.

The figure below illustrates the discovered quarks and leptons until now.

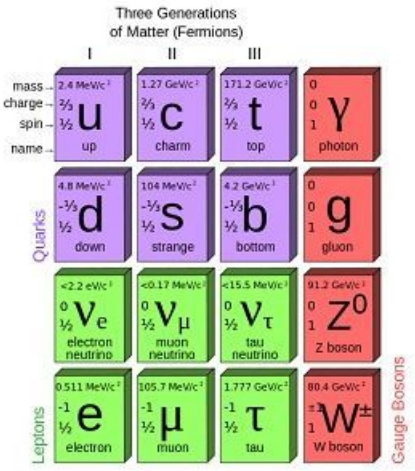

Figure 1: List of the fundamental particles [2]

To see in this scheme are also the gauge bosons. With exception of the Higgs boson, the three other bosons listed are the so called force carriers. The photons are responsible for the electromagnetic interaction, the W and Z bosons for the weak interaction and the gluons for the strong interaction [1].

The strongest force of the three (and also stronger than the gravitational force) is, as the name says, the strong force. It has, although, a small interacting range. This interaction is described by a quantum field theory called Quantum Chromodynamics (QCD). The section below will elucidate some points of this theory, giving more informations about the strong force.

1.2 Quantum Chromodynamics and the Quark-Gluon Plasma

The strong force has the interesting property of acting stronger on larger rather in smaller distances within the interaction range [3], different from the three other known forces. This feature, together with an energy dependence, gives the QCD theory two main characteristics: the quark confinement and the asymptotic freedom of particles.

Given the fact that the strong force is more active for larger distances, the required energy to separate quarks inside a hadron increases with the distance between them. The distance between bound quarks reaches an unsustainable point in which a quark-antiquark pair creation is more advantageous than the separation itself [4]. This property leads to a confinement, in which the quarks cannot escape from the original hadron [5].

In opposition to the confinement, another QCD property is detected when the hadrons are, for example, present in a high energy and temperature regime. Under these conditions, quarks can be detected as free in a dense matter called the Quark-Gluon Plasma (QGP). The QGP can be obtained for example in high energy collisions, where the energy density is so high and the separation between the quarks so small that the interaction between them in one hadron turns weak, making it possible for them to escape. The QGP formation happens in a phase transition, demonstrated on the image below:

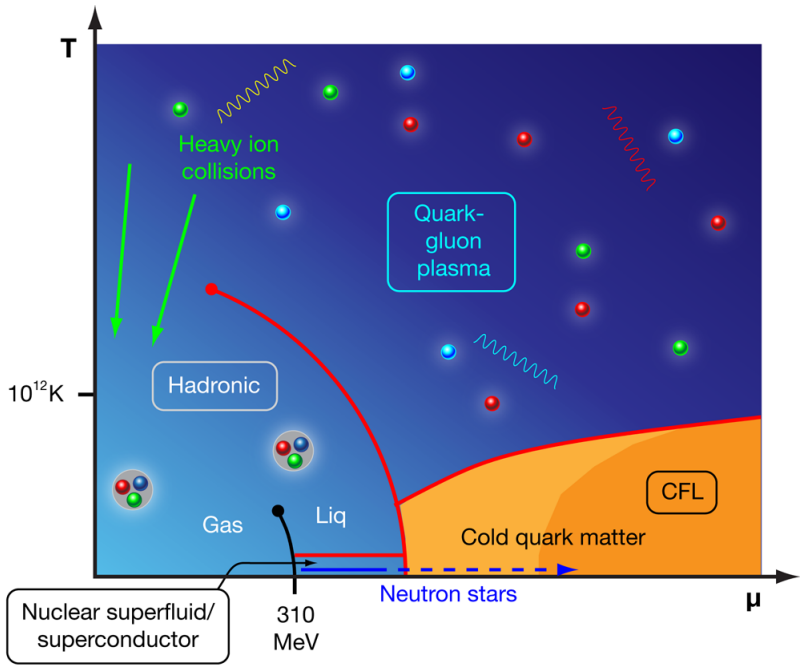

Figure 2: QGP phase diagram [6]

The diagram in the figure 2 shows the relation between the temperature T and μ, the baryo-chemical potential. The endpoint of the red line to the left represent the possible point in which the first transition would happen. CFL means Color-Flavor-Locked, a quark matter found in neutron stars at low temperatures. The region above the red line is the QGP, phase of matter already reached at high energy collisions [7].

1.3 Photon Interactions with Matter

Photons are particles without mass, which travel with a constant speed c when in vacuum. Also called gammas, the photons have no charge. Energy loss processes for the γ are therefore different when compared with charged particles, since it can't have any Coulomb interaction.

The possible energy loss mechanisms happen when a photon interacts with a medium and deposits its energy on it. There are three main different ways for the γ to interact with matter [8]:

- Photoelectric effect
- Compton effect
- Pair production

All these possible interactions depend highly on the photon energy at the moment when it crosses the material and also on the material composition, since the interaction depends on its atomic number. The next figure illustrates the total photon cross section versus its energy when travelling through materials made of carbon and lead, respectively.

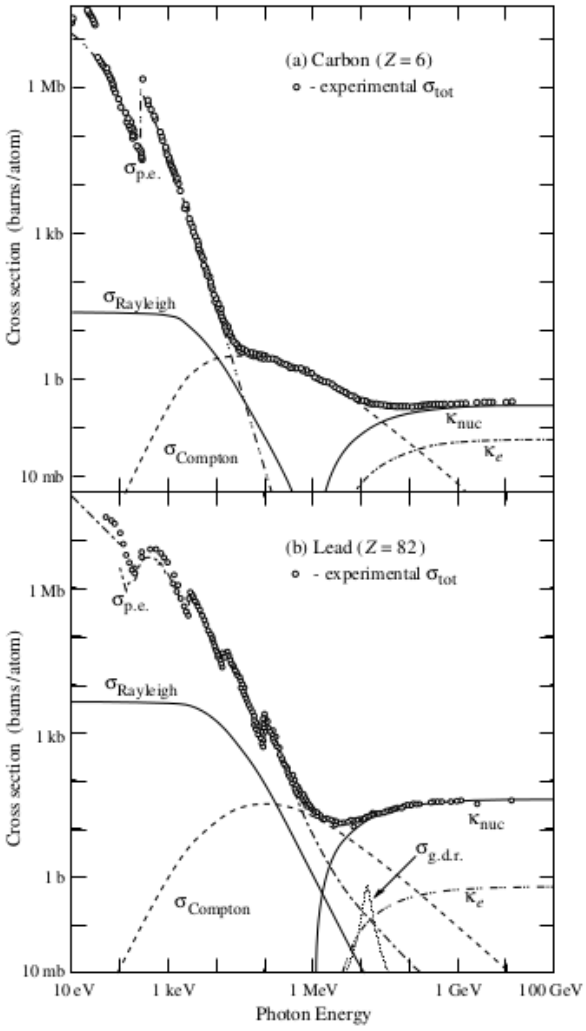

Figure 3: Total photon cross sections for different elements [9]

In the figure 3, $\sigma_{p.e.}$, $\sigma_{Compton}$ and κ_{nuc} represent the photon cross sections for the photoelectric effect, the Compton effect and the pair production in the nuclear field. The κ_e represents the photon cross section for pair production in the electron field and $\sigma_{Rayleigh}$ the photon cross section for the Rayleigh effect [10], that produces light scattering when photons interact with particles with smaller wavelenghts.

1.3.1 Photoelectric Effect

The photoelectric effect was explained by Albert Einstein in 1905 and rendered him the Nobel prize in 1921. This effect is observed when one photon with a kinetic energy of E = $h\nu$ is absorbed by the material through which it is travelling, most precisely by one bound electron of the material. In this process, all the γ energy is transferred to the electron, and the lepton will be then ejected from the atom [8], with an energy of:

$$E_{kin} = h\nu - E_b \tag{1}$$

Where E_b is the binding energy from the electron with the nucleus.

The photoelectric effect is the dominant energy loss process for a γ energy until approximately 100 keV.

1.3.2 Compton Scattering

The Compton scattering rules the most interactions in a medium/high photon energy range, between 100 keV and 1 MeV. This typical energy range shows that the Compton effect happens most with photons coming from radioisotope sources [11].

In this case, one photon incides in an electron of the material, transferring only a part of its energy. After interacting, the electron is deflected by an angle θ of its travel direction [12]. This deflection also causes an increase of the photon wavelength, given by the equation:

$$\lambda' - \lambda = \frac{h}{m_e c}(1 - cos\theta) \tag{2}$$

1.3.3 Pair Production

The pair production is one consequence of the photon interaction with matter when the γ energy $E_\gamma > 2m_e c^2$, i.e. $E_\gamma > 1.02$ MeV. When one photon with the enough mentioned incoming energy encounters the material and enters the Coulomb field of a nucleus, it can produce a e^+e^- pair and then disappear. It won't be found anymore because all of its energy converts to the lepton pair energy (rest and kinetic) [13]. The pair production is the most dominant effect in the high energy physics, and will be then the only effect considered for this task.

1.3.4 Bremsstrahlung

After one pair production, electrons can interact with matter causing Bremsstrahlung. When electrons pass through one material, they can be influenced by the Coulomb field of a nucleus and have its trajectory deflected. When this happens, they lose energy through radiation, the so called Bremsstrahlung. This effect happens more commonly for high energies.

1.4 The Omega(782) Meson

Discovered in 1961 at the Berkeley laboratory, the ω meson is a light unflavoured and a vector meson [14]. Vector mesons are mesons with spin 1 and odd parity. The omega quantum numbers are then $I^G(J^{PC}) = 0^-(1^{--})$.

Since the relativistic quark model development, by S.Godgfrey and N.isgur [15], it's known that, with a heavy quarks exception, there are nine possible combinations of $q\bar{q}$ [16]. These combinations are divided in groups called octets and singlets. If the heavy flavour decomposition for a pure singlet has a null isospin ($I = 0$), than one of the two possible physical states for this ($I = 0$) can be pure. This is true for the omega case. The ω is simply a pure state with no strange quarks, with $\frac{(u\bar{u}-d\bar{d})}{\sqrt{2}}$.

Its rest mass is, according to the PDG particle listings, of (782.65 ± 0.12) MeV/c^2. The omega has as most common decay channels [17]:

- $\pi^+\pi^-\pi^0$, with a branching ratio BR = (Γ_j/Γ) of $(89.2 \pm 0.7)\%$

- $\pi^0\gamma$, with a branching ratio BR = (Γ_j/Γ) of $(8.28 \pm 0.28)\%$

The most common decay will be the basis for this analysis.

1.5 High Energy Physics Quantities

In the high energy physics domain, some different spatial coordinates are used in addition to the commonly used ones. The pseudorapidity and the rapidity are used in hadron collider physics. The rapidity is a quantity defined by:

$$y = \frac{1}{2} \ln \frac{E + p_z c}{E - p_z c} \tag{3}$$

In this formula, y is the rapidity, E the energy of the particle and p_z its momentum on the z-direction.

For the comprehension of the meaning of this formula, one must observe two different cases. When one particle travels perpendicular to the z-direction (equivalent to the beam axis in the collision system), its momentum in this direction will be zero, turning the term inside the logarithm to one. The rapidity will then be zero. Considering the opposite case in which the particle travels parallel to the z-axis, the energy will be comparable to $E = p_z c$ and the rapidity will be infinite. Concluding, the rapidity will be dependent of the angle between the total momentum direction and the beam axis, growing bigger when this angle tends to zero [18].

The use of this quantity is usefull because the difference between the rapidity of two particles after a collision turns out to be the same as before the collision using Lorentz transformations i.e. it's constant. The disadvantage of the rapidity measurement for the high collider physics is the difficulty in measuring all the needed parameters. This problem leads to a definition of another variable, the pseudorapidity η.

To find the pseudorapidity, the rapidity energy term is calculated with the total momentum of the particle and must then be linearly expanded. After this expansion, the ratio between the momentum in the z-direction and the total momentum is made and denoted as the angle θ between the particle trajectory and the beam axis. The pseudorapidity term will be then:

$$\eta = -\ln \tan \frac{\theta}{2} \tag{4}$$

For relativistic particles, the rapidity and pseudorapidity will converge.

2 The Large Hadron Collider (LHC)

The Large Hadron Collider (LHC) is the largest particle collider in the world, located at CERN, in Geneva. The LHC, built inside the tunnel previously used for the LEP (Large Electron-Positron Collider), has the form of a ring with 27 km circumference and was built approximately 100 m below the surface [19]. The ring is formed by superconducting magnets maintained at a low temperature near the absolute zero (-271.3^{o}C). These magnets will create a strong magnetic field responsible for guiding particle beams in opposite directions until they collide.

Before entering the LHC, 2808 particle beams produced by hydrogen ionization or lead nuclei are first accelerated by a linear accelerator (LINAC) that uses radiofrequency. This method consists of waiting for radio waves to reach their peak, so that the associated electrical field can boost the particles. In sequence, after the beams reach enough energy, they are sent to two ring-shaped accelerators (PS - Proton Synchroton and SPS - Super Proton Synchroton). These two accelerators give a new boost to the particles, until they reach enough energy to enter the LHC [20].

As the particle beams enter the LHC with an injection energy of 0.45 TeV, they are accelerated by radiofrequency cavities, reach the desired center-of-mass energy and travel constantly until they collide. The collisions can happen at four different detectors, according to the main goal of the collision. The four detectors are:

- ATLAS (A Toroidal LHC Apparatus) [21] The ATLAS detector was built for the search of new particles and for a physics beyond the Standard Model. In 2012, ATLAS revealed the discovery of the Higgs boson, which was its main purpose. ATLAS also seeks for extra dimensions and origin of the dark matter.

- CMS (Compact Muon Solenoid) [22] CMS is one main-purpose detector at CERN together with the ATLAS detector. It has the same goals as ATLAS, but was built with a different technology and magnet system. It was also responsible for finding the Higgs boson in 2012.

- ALICE (A Large Ion Collider Experiment) [23] The aim of ALICE is the investigation of strongly interacting matter under extreme conditions. It analyses the Quark-Gluon Plasma.

- LHCb (Large Ion Collider beauty) [24] LHCb is the detector at LHC responsible for the studies of antimatter. This investigations are carried out with the analysis of the beauty quark.

The figure 4 illustrates the CERN complex with its different accelerators and sectors. The direction of travel of the protons and ions is also illustrated.

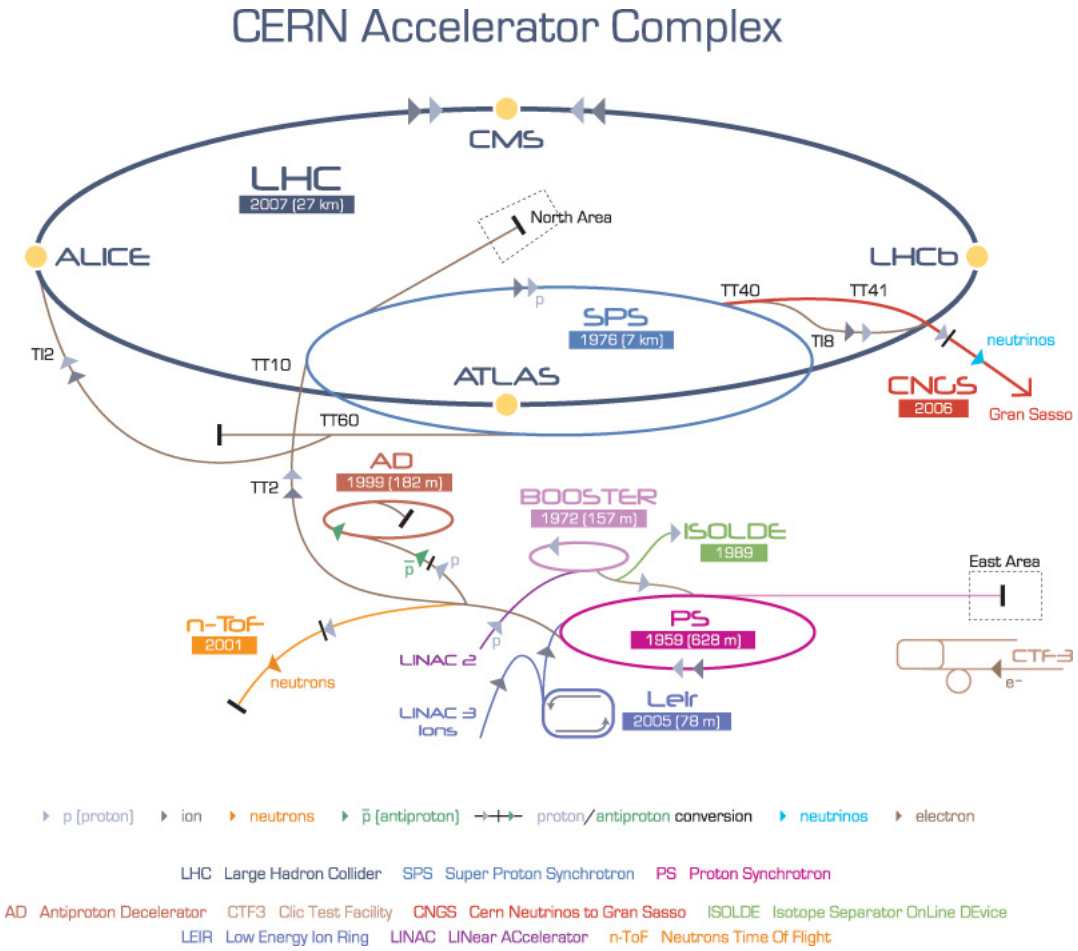

Figure 4: The CERN sectors and accelerators [25]

3 The ALICE Experiment

3.1 Introduction

ALICE (A Large Ion Collider Experiment) is one of the four major experiments at the LHC, designed for heavy nuclei interactions research at high energy densities. ALICE analyses data taken from particle collisions with a very good tracking and particle identification even in high particle density environment. It also explores a low transverse momentum region, different from another detectors. Due to these capabilities, the study of a new phase of matter, the Quark-Gluon Plasma (QGP), is possible.

In order to understand the underlying collision dynamics for the heavy ion collision and to control data for reference [26], the ALICE experiment also analyses proton-proton (pp) collisions.

The detector is composed by several detectors, each one of them having a task at identifying and studying the properties from the collision. Through these observations it is possible to infer the particle features, like momentum, mass, energy, etc.

The ALICE detectors are immersed in a magnetic field. This magnetic field bends tracks of charged particles, helping at the identification process: particles with high momentum, due to the high velocity, are practically not bent, whereas particles with low momentum are.

3.2 The Detectors

The ALICE experiment has seventeen different detectors [26], classified in three categories:

- Central Barrel Detectors

  Built inside a large solenoidal magnet, all of them are embedded in a magnetic field of B = 0.5 T. The set of the central barrel detectors is composed of:

  - The Inner Tracking System (ITS): has as a main task detecting low p_t particles and determining the primary vertex.
  - The Time Projection Chamber (TPC): is the main tracking detector at the ALICE experiment, which measures charged particles momentum. It has also a great particle identification capability based on the different particles' ionization.
  - The Transition Radiation Detector (TRD): is responsible for electron identification in a higher momentum range.
  - The Time of Flight Detector (TOF): identifies particles in an intermediate p_t range via the particles' time-of-flight measurement.
  - The Photon Spectrometer (PHOS): measures electromagnetical signals.
  - The Electromagnetic Calorimeter (EMCal): is qualified to identify neutral particles (more efficiently when they are high energetic). It also contributes with high momentum electrons measurement and analyses jet interactions for heavy ion collisions.
  - The High Momentum Particle Identification Detector (HMPID): detects charged particles with high momentum which cannot be identified by another ALICE detectors.

  Their design coverages are written on the table below. In this table, η is the pseudorapidity range coverage and ϕ is the azimuthal coverage. It's important to say that not all TRD and PHOS modules were installed for the ALICE Run 1 and the real phi coverage was therefore different.

Table 1: ALICE Central Barrel Detectors Coverage [12][26][27]

Detector	$\pm\eta$	ϕ	Radial Position	
ITS:				
SPD (1/2)	2	$0^o < \phi < 360^o$	3.9/7.6 cm	
SDD (1/2)	0.9	$0^o < \phi < 360^o$	15.0/23.9 cm	
SSD (1/2)	0.97	$0^o < \phi < 360^o$	38/43 cm	
			Inner Radius	Outer Radius
TPC	0.9*	$0^o < \phi < 360^o$	84cm	246,6cm
TRD	0.84	$0^o < \phi < 360^o$	290cm	370cm
TOF	0.9	$0^o < \phi < 360^o$	370cm	399cm
PHOS	0.12	$220^o < \phi < 320^o$	460cm	478cm
EMCal	0.7	$80^o < \phi < 187^o$	430cm	455cm
HMPID	0.6	$1.2^o < \phi < 58.8^o$	490cm	

* For full radial track length

- Forward Detectors
  - The Photon Multiplicity Detector (PMD): evaluates photon multiplicity and distribution.
  - The Forward Multiplicity Detector (FMD): analyses multiplicity distributions.
  - V0: provides the Minimum Bias trigger, estimates the centrality of Pb-Pb events and the multiplicity for p-Pb collisions.
  - T0: measures the vertex of the collision, grants a L0 trigger and gives a timing signal with the real time of the collision.
  - The Zero Degree Calorimeter (ZDC): calculates the energy of incoming nucleons, which carry informations about the collision.
- Muon Spectrometer

  The MUON spectrometer is used to measure high p_t muon pairs from the quarkonia decay at a pseudorapidity range of $2.5 < \eta < 4.0$.

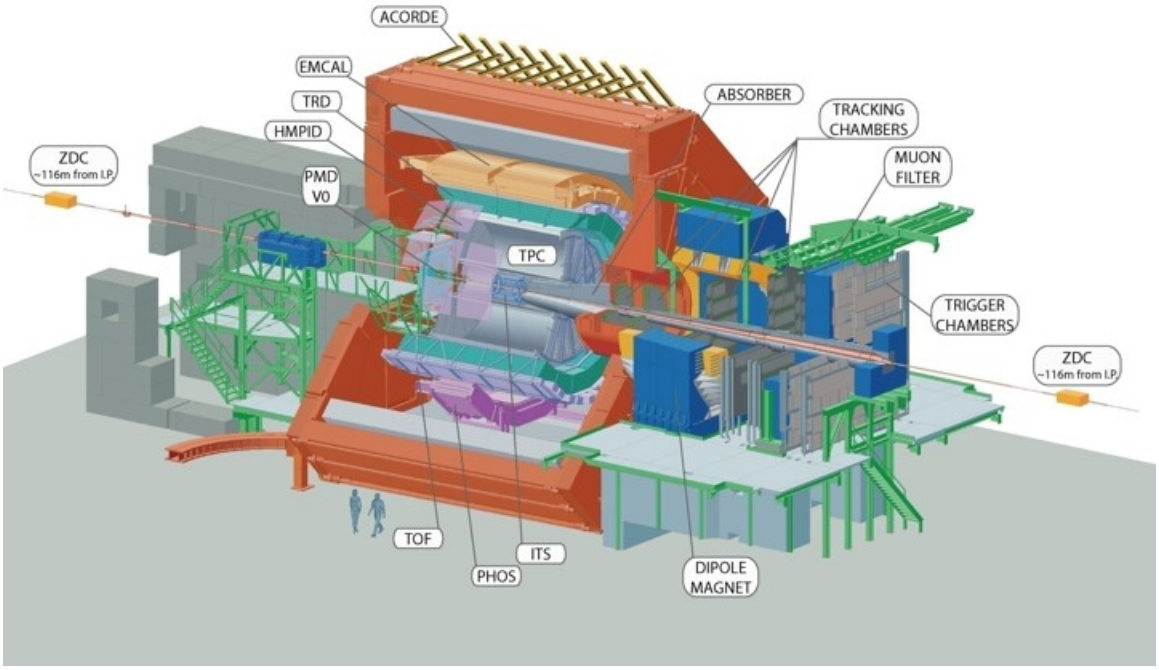

Figure 5: The ALICE Experiment setup during Run 1 [28]

Not all of the detectors listed above have an important role for this omega analysis. Hence, only the relevant ones will be explained in the next subsections.

3.3 The Inner Tracking System

The Inner Tracking System (ITS) [26] is the ALICE most internal detector, constituted by six silicon layers. Their assignments change every two layers, where different technologies are applied. These three systems, with two layers each, are (from the inside to the outside) made of:

- Silicon Pixel Detectors
- Silicon Drift Detectors
- Silicon Strip Detectors

The figure 6 illustrates the ITS design. The two internal orange layers compose the SPD, the blue ones illustrate the SDD and the purple external layers represent the SSD.

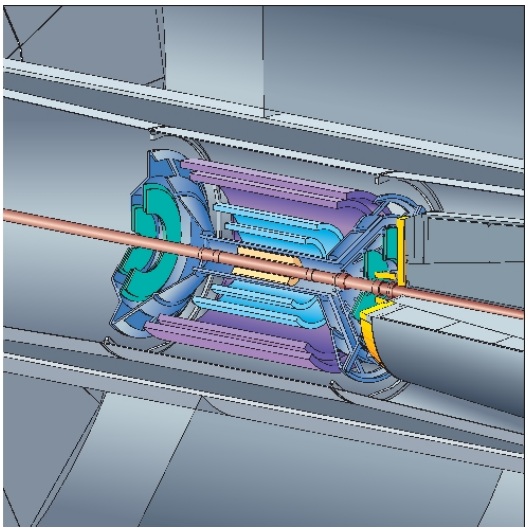

Figure 6: ITS layers scheme [28]

The ITS is responsible for the distinction between the primary vertex and secondary vertices created by short lived particles [29], and consequently for the primary vertex reconstruction. The first layers of the ITS must have a good resolution power in order to capture the large number of events near the collision point for the primary vertex definition. The adjacent layers will focus more on the track finding (for particles with low momentum), contributing with the ALICE global tracking.

3.3.1 The Time Projection Chamber (TPC)

The Time Projection Chamber (TPC) [26] is a cylinder-shaped and also the main tracking detector of ALICE, which gives information about the charged particles created in the collision.

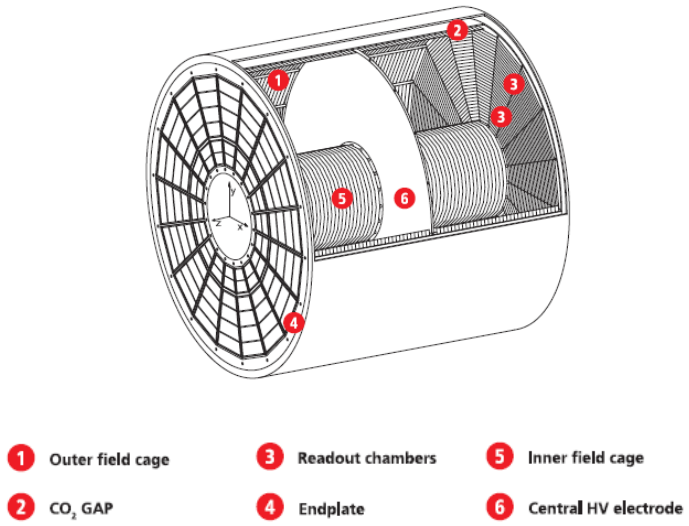

Figure 7: The ALICE Time Projection Chamber [30]

With 90 m^3, the TPC is divided in two parts by a central (drift) electrode and filled with gas (composed of Ne and 10% of CO_2). When the incoming particles from the collision encounter the gas, it ionises creating ions and electrons. The electrons from the ionized gas will drift in the direction of the positive endplates and produce signals [30]. These signals are used to calculate the specific ionization, also called dE/dx measurement, used to identify particles with the TPC. This energy loss measurement is described by the Bethe-Bloch formula [12], where:

$$-\frac{dE}{dx} = Kz^2\frac{Z}{A}\frac{1}{\beta^2}\frac{1}{2}\ln\frac{2m_ec^2\beta^2\gamma^2T_{max}}{I^2} - \beta^2 - \frac{\delta}{2} \tag{5}$$

In this equation: Z is the atomic number, A the atomic mass, $\beta = (v/c)$ the velocity of the electron, m_e the electron mass, c the speed of light, I the medium's ionization potential, $\gamma = \frac{1}{\sqrt{1-(\frac{v}{c})^2}}$ the Lorentz factor and T_{max} the maximum energy transfer. The parameter K depends on the detector materials and on the Avogadro constant (N_A):

$$K = 4\pi N_A r_e^2 m_e c^2 \rho z^2 \tag{6}$$

Different particles will have specific energy losses in the TPC, producing different Bethe-Bloch curves, showed below:

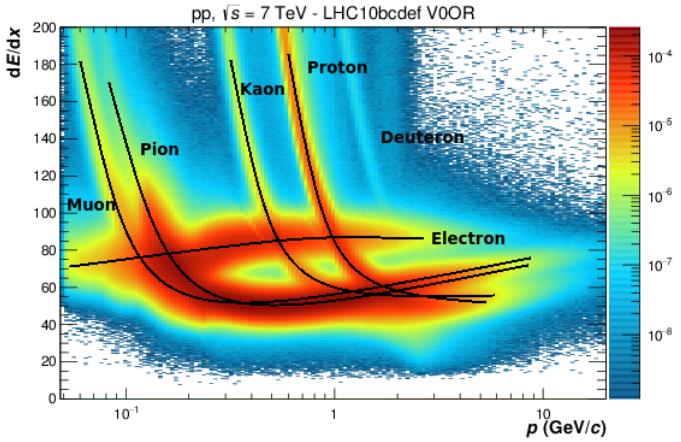

Figure 8: Energy loss curves for different particles

Observing the diagram, one can see that this method has a powerful PID (Particle Identification), although with a better resolution for a low p_t range. The reason for that is that the energy loss is inversely proportional to the β^2 parameter. Curve intersections happen more frequently above a certain momentum range, turning the energy loss measurement alone insufficient for the PID.

3.3.2 The Electromagnetic Calorimeter (EMCal)

The EMCal is located inside the solenoidal magnet of ALICE, and evolves the TPC detector with an azimuthal coverage of 107 degrees. It covers a pseudorapidity range of $|\eta| < 0.7$, allowing a back-to-back coverage with the PHOS detector [31].

The EMCal's basic structure is an arch of Super Modules (SM), each one containing small and identical detector units called modules, with four independent towers each. The modules are made of alternating plastic scintillator and lead layers. When one particle interacts with the lead layer, it deposits all its energy in different but neighbour cells. To this signal in different cells will be given the name "cluster". The interaction will create an electromagnetic or hadronic shower, releasing several electron-positron pairs and photons. Those particles will subsequently loose energy and produce another secondary particles when trespassing the other lead layers. All these particles are detected

in the plastic scintillator layers and transformed into electrical signal, which gives then informations about the energy their energy.

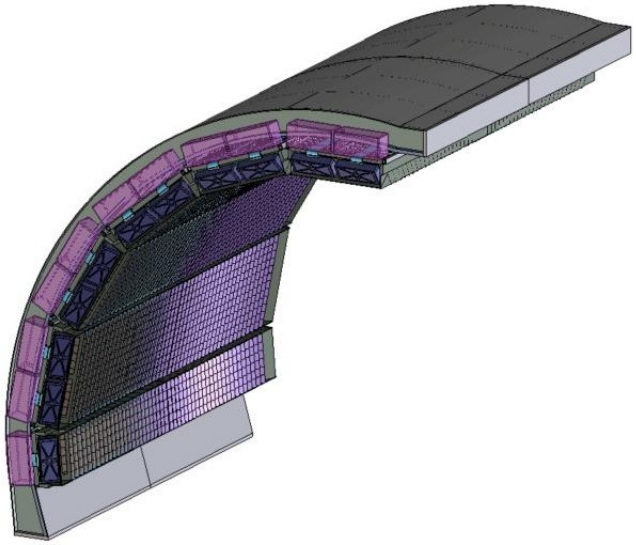

Figure 9: The Electromagnetic Calorimeter with its supermodules [31]

Although the EMCal has a great capability to reconstruct large p_t jets and identifies high momentum electrons, it is also used to identify photons and neutral mesons such as the π^0.

3.3.3 V0 Detector

The V0 detector [26][32] is formed by two detector arrays, the V0A and the V0C, located at opposite sides of the ALICE detector. The distance between each one and the collision point is different, and they cover also different pseudorapidity ranges. The V0 detector contributes to the event centrality determination and also detects charged particles. The V0 detector provides also Minimum Bias triggers with the possible configurations V0OR and V0AND. V0OR requires information from at least one of the arrays and V0AND from both.

The image below shows the V0 detector. The beam axis is represented by z and the y axis is aligned to the collision point in the radial direction. The V0A and V0C detectors are also represented, with different distances and in opposite sides of the collision point.

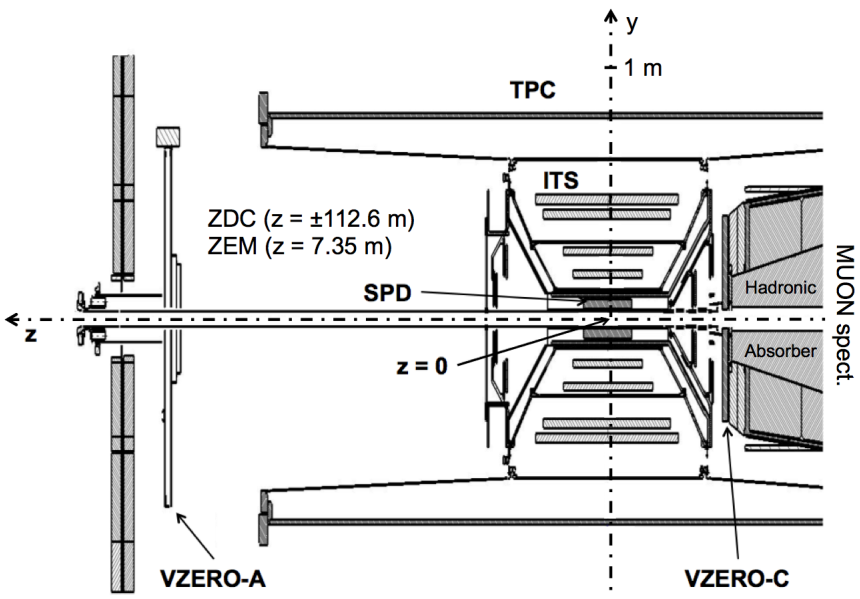

Figure 10: V0A and V0C positions [33]

The Minimum Bias Trigger

Different from another triggers, with the example of the EMCal trigger, the Minimum Bias Trigger doesn't require determined conditions for the final state [34]. It will take the largest possible number of events [32] and this difference will end up selecting more events with low multiplicity and low p_t, more common in such collisions [34].

4 Analysis Framework and Data Analysis

4.1 The AliRoot Framework

Built specially for the ALICE Experiment, the AliRoot Framework can analyse the physical events behind data and simulated collisions. It contains all the ALICE detectors information and can therefore simulate how they work, obtaining their results. Used for analysis, reconstruction and simulation, AliRoot is based on the ROOT scientific software framework, which is based on the C++ language. It was also developed at CERN, for the study of high energy physics [35]. The AliRoot Framework, together with ROOT, will be used for the data investigation in this analysis.

4.2 The Neutral Pion Reconstruction

The omega will be reconstructed in this analysis via its main decay, $\omega \rightarrow \pi^+\pi^-\pi^0$. This decay channel requires in the first place all pions' detection, starting with the neutral pion.

The π^0, being a light meson, decays too fast after its creation at the collision. For this reason, it cannot be directly measured by any detector and claims a reconstruction. This reconstruction can be executed with the use of two different methods: The Photon Conversion Method or the EMCal Clusters Analysis. These two modes are clarified in the sections below.

Before that, it is important to know that the neutral pion's most common decay is in two photons $\pi^0 \rightarrow \gamma\gamma$, with a branching ratio of $(98.823 \pm 0.034)\%$ [36]. It can also decay in other ways, but they will not be considered for this analysis.

This task presents only statistical errors. Therefore, systematic errors need to be analysed in the future for a concrete error definition.

4.2.1 Neutral Pion Reconstructed via EMCal Clusters

The distinction of the different particles detected by EMCal and their subsequent classification as leptons, photons or hadrons is essentially based on three basic steps [37]:

- Measurement of the energy deposited on the cluster together with the verification if there is a match between the analysed cluster and a TPC track. If not, the track absence indicates that the particle in question has no charge.
- Analysis of the particle time-of-flight cluster information. Hadrons can be distinguished from leptons because they are heavier and therefore slower.
- Observation of the cluster shower shape parameters. This parameters characterize the clusters and each cluster has a different pattern for every particle type. Hadronic and electromagnetic showers produce different shower patterns and can be identified by their parameters.

The EMCal shower shape parameters are portrayed in the image below:

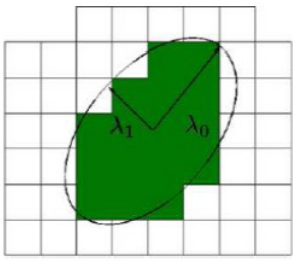

Figure 11: Shower shape parameters [38]

The values of the parameters are given by the following equations [38]:

$$\lambda_0^2 = M_{02} = \frac{d_{xx} + d_{zz}}{2} + \sqrt{(\frac{d_{xx} + d_{zz}}{2})^2 + d_{xz}^2} \tag{7}$$

$$\lambda_1^2 = M_{20} = \frac{d_{xx} + d_{zz}}{2} - \sqrt{(\frac{d_{xx} + d_{zz}}{2})^2 + d_{xz}^2} \tag{8}$$

The analysis via shower shape is based on the theory of probabilities, and the λ_0^2 is taken as the distinguishing parameter. In the formula presented above d_{xx}, d_{zz} and d_{xz} are the variances normalized to the cell weight [38].

A good π^0 reconstruction via EMCal clusters depends on the analysed p_t range. For a low/intermediate transverse momentum range with $1.0 < p_t < 5.0$ GeV/c, the two decay photons will produce distant EMCal signals and their corresponding clusters will be therefore distinct. These signals will start to merge at a $p_t = 5.0$ GeV/c and produce nearer cluster pairs. This proximity will reach a point at a $p_t = 10.0$ GeV/c in which the merged clusters predominate [39].

The left image in the figure 12 illustrates the opening angle of two decay photons in a Pb-Pb Monte Carlo collision. The black, blue and green lines represent the opening angle of one, three and five EMCal cells, respectively [39]. The vertical line shows the point where the clusters start to merge. The right image shows a simulation result that indicates the point from which the presence of two photons in one same cluster will predominate, relating the percentage of one or two photons in the clusters to the energy of these photons.

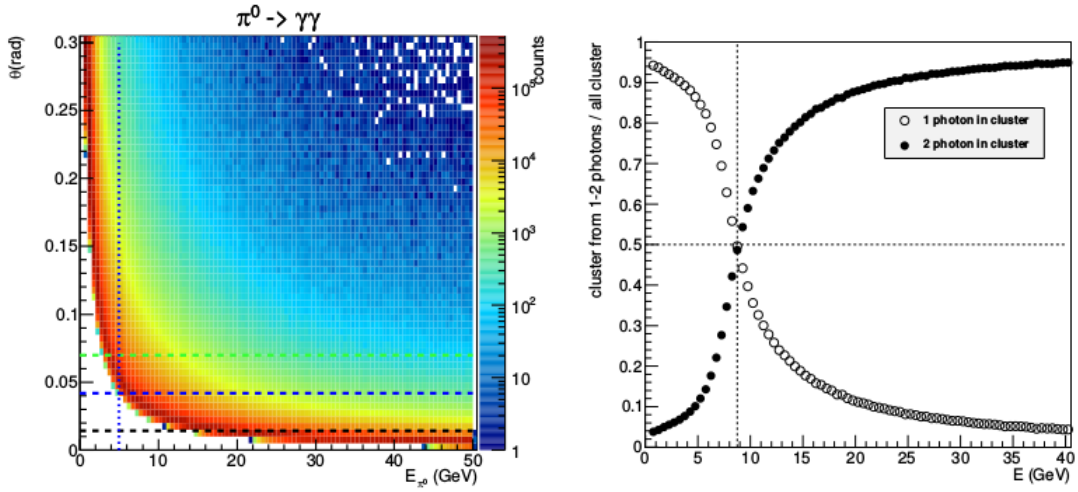

Figure 12: Decay photons opening angle and percentage of one or two photons in the clusters [39]

This transverse momentum dependence will then require an accurate PID analysis.

As said above, the π^0 is easily detected for a $p_t > 10$ GeV/c, as most clusters converge becoming one, reproducing a larger parameter value. For a smaller traverse momentum, the shower shape study won't be enough and will require a invariant mass analysis.

The invariant mass analysis takes place after all the decay photons' distinction. The first step of this process is the investigation of all possible $\gamma\gamma$ pairs, given by the combination of two different photons from the same event. This permutation is made for all the photons and will contain informations like energy and mass of both particles that will be substituted in the invariant mass formula, as described below, with α being the angle between the associated photons:

$$m_{\gamma\gamma} = \sqrt{E_{\gamma 1} E_{\gamma 2} - p_{\gamma 1} p_{\gamma 2} \cos(\alpha)} \tag{9}$$

The formula results will be read as outputs to produce a signal, captured in one histogram. The histogram will have a gaussian form with a peak at the π^0 mass and also a combinatorial background, which exists due to $\gamma\gamma$ combinations that don't represent a π^0 meson. This histogram can be seen below:

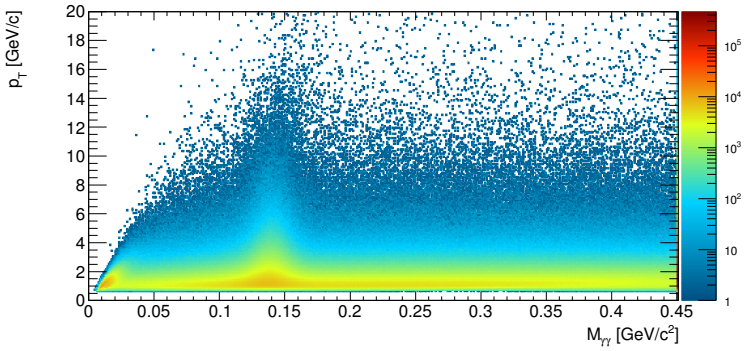

Figure 13: $M_{\gamma\gamma}$ invariant mass plot with pure EMCal reconstruction in pp collision at $\sqrt{s} = 7$ TeV - LHC10bcdef

Now that the histogram is made, one must now subtract all the generated combinatorial background. This is accomplished by a process that excludes all the possible wrong combinations, called the Event Mixing technique. Since the omega background subtraction is done the same way, more explanations can be found in section 7.2. It is important to understand that the considered particles and associations will be different for the omega and the neutral pion, due to their different decays.

The final step is the gaussian fit. This function will reproduce the peak and its parameters will give the encountered neutral pion mass with the associated errors.

4.2.2 Neutral Pion Reconstructed via Photon Conversion Method

The Photon Conversion Method considers the fact that γ particles can produce electron-positron pairs after interacting with the detector material, more precisely with its nuclei Coulomb fields (see section 2.3.3). The neutral pion reconstruction is then, in this case, based on these two leptons' track finding and association. Since the photon cross section is different for different elements (see figure 3), a good knowledge of the material properties is required to the comprehension of this pair production effect.

The search for this electron-positron pairs starts with all the ITS and the TPC measured tracks. One algorithm called V0 Finder will be used to combine these tracks in pairs and determine their vertex, when those have more then 0.5 mm distance from the primary vertex. These vertices will be submitted to the requirement that both tracks must have a maximal distance of 1.5 cm between them in their origin [37], in order to exclude tracks that weren't correlated. When this cut is applied, the vertex is called a V0 candidate, i.e. a secondary vertex candidate. After all improvements, the encountered vertex is said to be a secondary vertex.

To find one electron-positron pair vertex, the secondary vertex is required to be between 0.5 cm $< r <$ 180 cm. Cuts are also applied for the TPC number of sigmas, in order to include only electrons and positrons tracks. The invariant mass of the electron and positron is calculated and subjected to cuts. The reconstructed photon momentum needs to point to the primary vertex, because the neutral pion decay happens too fast after the collision.

This process is illustrated in the next image:

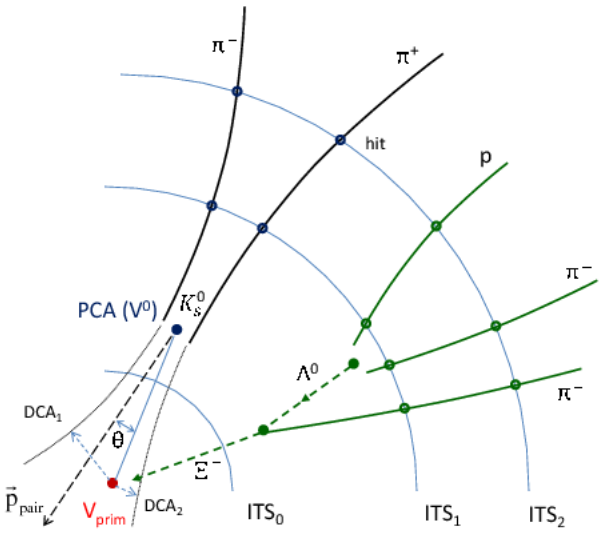

Figure 14: V0 candidate reconstruction procedure [37]

Having one encountered gamma candidate, one can now do an invariant mass plot, associating it with another photon. This another γ can be simply a EMCal cluster or another photon reconstructed by the PCM. It is important to remark that the possibility of two photons from the same π^0 mother to decay is much smaller than finding two gammas from EMCal clusters and also smaller when the reconstruction is based on one EMCal cluster and one conversion photon. The accuracy with pure PCM is although better, due to the good ALICE capability in track finding and to the EMCal bad resolution in a low momentum region. The only problem for PCM is the lack of statistics at a high transverse momentum. Below, a neutral pion invariant mass histogram for pure PCM is plotted.

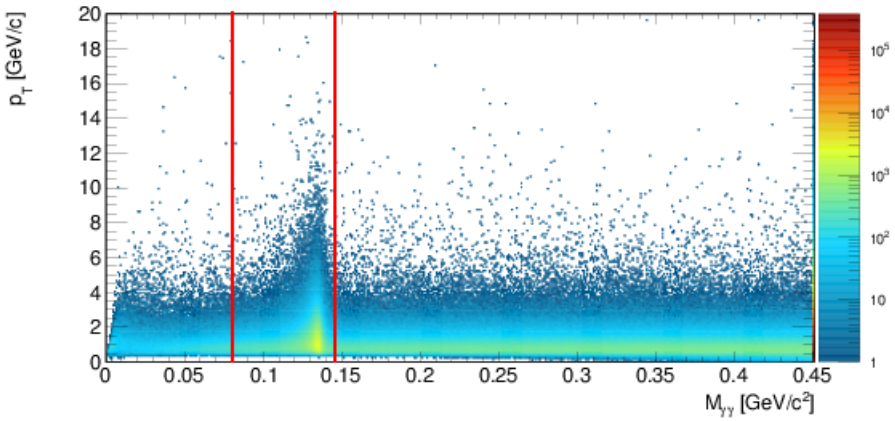

Figure 15: $M_{\gamma\gamma}$ invariant mass plot with pure PCM reconstruction in pp collision at $\sqrt{s} = 7$ TeV - LHC10bcdef

Comparing this histogram with the one in figure 13, one can see that the number of entries is smaller, although the neutral pion peak identification is easier.

4.3 Data and Event Selection

This omega analysis will use LHC pp collisions data from the year 2010, with a center of mass energy of 7 TeV. The data sample contains only Minimum Bias events from the LHC10b, LHC10c, LHC10d, LHC10e, LHC10f periods. Only pass 4 data has been analysed. Altogether, there were 410 million MB events used.

The search for the omega meson begins with the event cuts. The next step is the search for gamma candidates. The task looks for them according to the determined neutral pion reconstruction configuration: pure PCM, pure Calorimeter or PCM-Calorimeter. This time, gamma cuts are implemented.

The analysis demands subsequently the charged pions detection, with the suitable detectors to find them. Cuts are made to energy loss measurements and other track and detector parameters.

The study can now reach its final purpose and examine omega candidates. For the last time, cuts are applied to the pions combination. At the end, there aren't only mesons to see. The presence of combinatorial background will require a background analysis and its future subtraction.

A final result for data will be obtained only when all these steps are concluded. The data results will include the omega raw yield, corrected only after the obtainment of MC simulation results.

4.3.1 Monte Carlo Simulations

Monte Carlo (MC) simulations are performed in this analysis for the finding of true omegas, which will be compared to the ones found in data. Only then it will be possible to see if the background was good described and suppressed. The MC results will also be necessary for the efficiency and acceptance calculation.

The MC simulation for this work uses Pythia 8. Pythia is an event generator based on the C++ language, responsible for the reproduction of high-energy physics events. Pythia operates in three different frames [40][41]:

- Process Level
- Parton Level
- Hadron Level

The Process Level is the class responsible for the main event definitions (often hard processes). The subsequent class, the Parton Level, reproduces partonic interactions, structure of beam remnants and radiation. The last class, the Hadron Level, will create hadrons from the partons and reproduce decays from more unstable particles. All the MC produced results will be treated as data, but now with the advantage that one can ask what particles are "true", i.e. the real produced particles.

4.4 Applied Cuts

For a successful analysis, different cuts were applied. Event, Conversion Photon, Pion, Neutral Pion and Meson Cuts were employed, and all of them will be listed in the subsections below.

4.4.1 Event Cuts

No multiplicity cuts were made for the events. All of the events were triggered by V0OR: in another case, they will be excluded. The pile-up is removed, and trigger signal if not from Minimum Bias will be discarded. There was also a Vertex Cut from $|z| < 10$ cm.

Table 2: Event Cuts

Cut Type	Option	Action
HeavyIon	0	pp collision mode
CentralityMin	0	0
CentralityMax	0	0
SelectSpecialTrigger	0	V0OR
SelectSpecialSubTriggerClass	0	none
RemovePileUp	1	Pile Up Removed
RejectExtraSignals	1	Only Minimum Bias Events
VertexCut	3	-10 cm < z Vertex < 10 cm

4.4.2 Photon Conversion Cuts

The conversion cuts were made in a way that the leptons can be identified only within the fiducial zone. The chosen V^0 algorithm operates during the collision, i.e. online. Particles are conversion candidates only if their position in the R direction is bigger than 5 cm, so that Dalitz photons are not detected. The lepton traverse momentum is required to be bigger than 0.05 GeV/c. The track identification in the TPC is made with a cut in the number of sigmas: for the electron the cut is $|\mathrm{n}\sigma\mathrm{ElectronTPC}| < 5$ and for the pion the cut is $-10 < \mathrm{n}\sigma\mathrm{PionTPC} < 0$. Another condition is the minimum of 60% of TPC findable clusters. After the combination of one positron and one electron, another cuts are also made for the cosine of the pointing angle and for the Armenteros-Podolanski plots. The pointing angle represents the direction of the particle's momentum. The Armenteros plot relates the transverse momentum Q_T of the positive daughter particle with respect to the mother particle momentum with the longitudinal momentum asymmetry [42]. The transverse momentum Q_T and the longitudinal momentum assimetry α are given by [42]:

$$Q_T = \frac{|\overrightarrow{p_T} \text{ x } \overrightarrow{p_m}|}{|\overrightarrow{p_m}|} \tag{10}$$

$$\alpha = \frac{p_d^+ - p_d^-}{p_d^+ + p_d^-} \tag{11}$$

In the asymmetry equation, $p_d^{\pm}$ are the momenta of the positive and negative daughters. The figure 16 shows the Armenteros plots before and after the cuts.

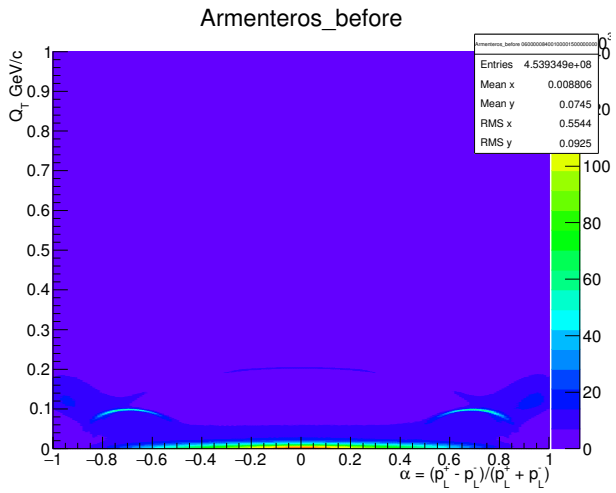

(a) Armenteros-Podolanski Before Cut

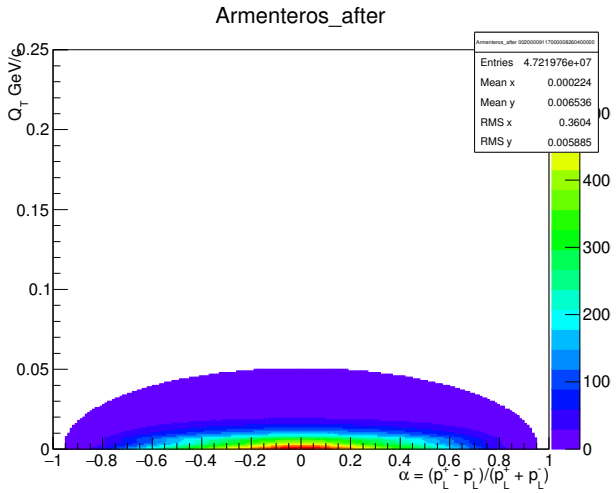

(b) Armenteros-Podolanski After Cut

Figure 16: Armenteros plot before and after Q_T cut

Table 3: Photon Conversion Cuts

Cut Type	Option	Action
V0FinderType	0	on-fly V0 type
EtaCut	0	$-0.9 < \eta < 0.9$
MinRCut	2	5 cm
EtaForPhiCut	0	Full eta range
MinPhiCut	0	No phi sector cut
MaxPhiCut	0	No phi sector cut
SinglePtCut	0	$p_t > 0.05$ GeV/c
ClsTPCCut	9	60% of findable clusters
ededxSigmaCut	1	$-5 <$ nσElectronTPC < 5
pidedxSigmaCut	1	$-10 <$ nσPionTPC < 0
piMomdedxSigmaCut	7	Min Momentum $n\sigma$ above the pion line = 0.4 GeV/c
piMaxMomdedxSigmaCut	0	No max momentum cut
LowPRejectionSigmaCut	0	No proton or kaon rejection
TOFelectronPID	0	No TOF electron cut
ITSelectronPID	0	No ITS electron cut
TRDelectronPID	0	No TRD electron cut
QtMaxCut	8	2D Q_T max cut for Armenteros = 0.05
Chi2GammaCut	2	χ^2 max cut = 30
PsiPair	6	Psi pair cut < 0.05
DoPhotonAsymmetryCut	0	No cut
CosinePointingAngle	4	$\cos\theta > 0.85$
SharedElectronCuts	0	No cut
RejectToCloseV0s	0	No cut
DcaRPrimVtx	0	No cut
DcaZPrimVtx	0	No cut
EvetPlane	0	No Event Plane

4.4.3 Pion Cuts

The applied pion cuts for this analysis are based on the TPC minimum clusters and on the number of sigmas in the energy loss histogram. Another consideration is that the invariant mass for one charged pion pair can't be greater than 0.75 GeV/c^2. There is also the requirement that the pion cannot have a transverse momentum lower than 0.1 GeV/c.

Table 4: Conversion Cuts

Cut Type	Option	Action
kEtaCut	0	No Eta cut
kClsITSCut	0	No ITS cluster cut
kClsTPCCut	2	Minimum clusters TPC = 80
kDCACut	0	Open cuts
kPtCut	1	0.1 GeV/c
kPiDedxSigmaITSCut	0	No cut
kPiDedxSigmaTPCCut	7	$-3 <$ nσTPC < 3
kPiTOFSigmaCut	0	No TOF Cut
kMassCut	2	0.75 GeV/c^2

The histograms below show two of the applied pion cuts:

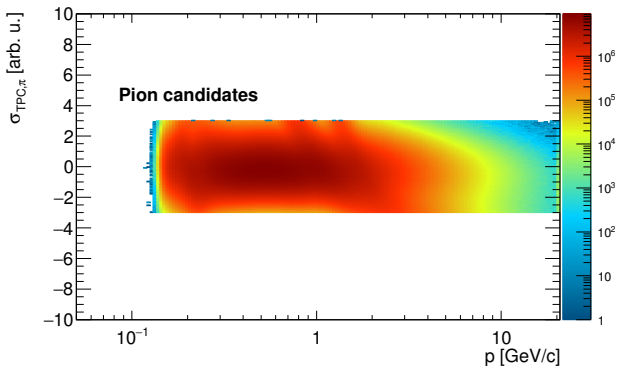

(a) Number of Sigmas Cut

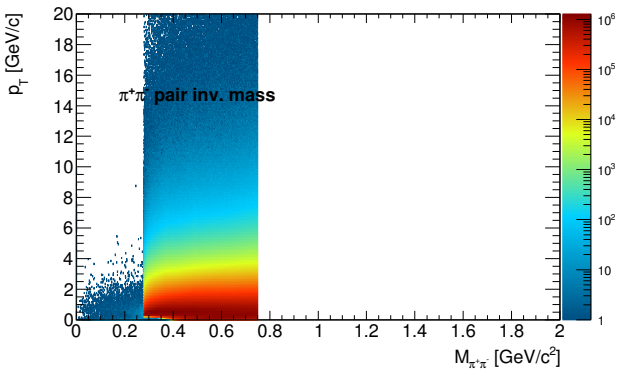

(b) $\pi^+\pi^-$ Invariant Mass Cut

Figure 17: Two applied pion cuts

4.4.4 Neutral Pion Cuts

The neutral pion cuts are based on the meson reconstruction and how the background is subtracted to find the signal (see section 7.2.). The background events in this case are limited to 5 and the background scheme is made using only the V0 multiplicity, without the track multiplicity. Although the maximal degree for rotation method is configured to be 20^o, this method won't be employed for this analysis. The r cut is large, and the rapidity is required to be smaller than 0.85. There aren't any shared electrons, opening angle, r and z primary vertex cuts. The Monte Carlo Smearing, used for Monte Carlo peak width corrections, wasn't applied and too close V0 candidates weren't rejected. The selection window is responsible for doing the cut on the π^0 invariant mass histogram, and is configured to be between 0.08 GeV/c^2 and 0.145 GeV/c^2.

Table 5: Neutral Pion Cuts

Cut Type	Option	Action
MesonKind	0	-
BackgroundScheme	1	Mixed event with V0 multiplicity
NumberOfBGEvents	0	5
DegreesForRotationMethod	3	20
RapidityMesonCut	5	y ¡ 0.85
RCut	0	$r < 180$ cm
AlphaMesonCut	3	$0 < \alpha < 1$
SelectionWindow	1	0.08 GeV/c^2 $< \pi^0$ Invariant Mass $<$ 0.145 GeV/c^2
SharedElectronCuts	0	No cut
RejectToCloseV0s	0	No rejection
UseMCPSmearing	0	No smearing cut
DcaGammaGamma	0	No cut
DcaRPrimVtx	0	No cut
DcaZPrimVtx	0	No cut
MinOpanMesonCut	0	No open angle cut
MaxOpanMesonCut	0	No open angle cut

4.4.5 Meson Cuts

The omega meson cuts differ from the neutral pion cuts only on the selection window, since the omega invariant mass cut is applied only in the signal extraction.

Table 6: Meson Cuts

Cut Type	Option	Action
MesonKind	0	-
BackgroundScheme	1	Mixed event with V0 multiplicity
NumberOfBGEvents	0	5
DegreesForRotationMethod	3	20
RapidityMesonCut	5	y ¡ 0.85
RCut	0	$r < 180$ cm
AlphaMesonCut	3	$0 < \alpha < 1$
SelectionWindow	0	No selection window cut
SharedElectronCuts	0	No cut
RejectToCloseV0s	0	No rejection
UseMCPSmearing	0	No smearing cut
DcaGammaGamma	0	No cut
DcaRPrimVtx	0	No cut
DcaZPrimVtx	0	No cut
MinOpanMesonCut	0	No open angle cut
MaxOpanMesonCut	0	No open angle cut

5 The Omega Analysis

5.1 Omega Reconstruction

The ω reconstruction needs, after the neutral pion reconstruction, the determination of the charged pions in the event. The π^+ and the π^- detection is made in this case by the TPC with the help of energy loss measurements and its appropriated cuts. After the charged pion candidates' definition, these are combined in pairs when originated from the same vertex and plotted in an invariant mass histogram. Cuts are furthermore applied.

Having these results, charged pion pairs are combined with the neutral pion candidates and a 2D invariant mass *vs.* p_t histogram is plotted.

The omega invariant mass plot is displayed below:

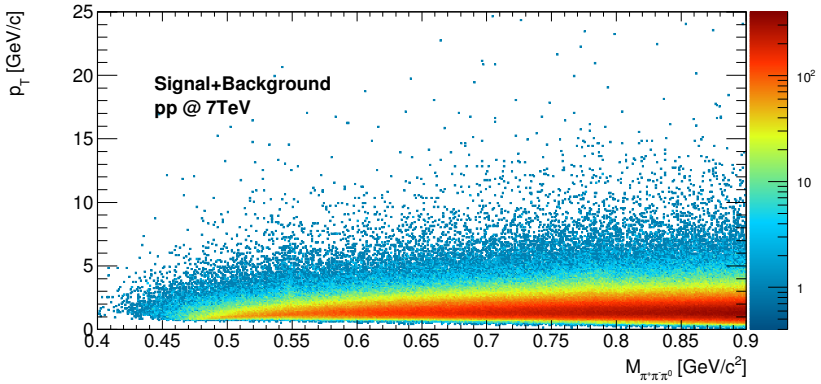

Figure 18: Omega Invariant Mass Plot

This histogram shows a large amount of background. In order to observe the real peak, the background needs to be well described and subtracted.

5.2 Background Description - Event Mixing

The background form is described by wrong $\pi^+\pi^-\pi^0$ combinations, since it is created by the different meson permutations that won't necessarily correlate and/or create a gaussian peak on the invariant mass histogram. The technique responsible for describing the background through combinations is the so called Event Mixing.

For the Event Mixing, all possible pion associations are divided in three main groups, disposed at the table below. To be sure that signal won't be subtracted, the three associated pions will never come from the same event. The Group 1 represents positive and negative pions coming from the same event, the second one speaks for the neutral and positive pions from the same event and the last group for the neutral and negative pions from the same event. In this table, E stands for an event. The i and j indices are used to express if the events are the same or not.

Table 7: Three Main Background Groups

Group	π^0	π^+	π^-
Group 1	E_i	E_j	E_j
Group 2	E_i	E_i	E_j
Group 3	E_i	E_j	E_i

These three groups contain all the necessary considerations to represent the background, since they consider all possible correlations:

- The two pions from the same event can be correlated or not,
- When the two pions are correlated, they can come from an omega or from another particle,
- The pion from the different event can come from one omega or not.

An important AliRoot tool will be employed to the background study with the Event Mixing technique: the Background Handler. The Background Handler is an AliRoot class, which has the necessary background calculation tools. It investigates the number of background events and distinguish meson events when they are added to the analysis. This investigation is made based on the vertex position in z and track multiplicity. Two background handlers were created for this analysis: one for the negative pion and one for the positive pion.

In this study, neutral pion candidates entries were fixed as the main event loop. Inside this loop were made two other loops, depending on the pion event, to associate the particles:

- Charged pions from the same event: positive pion handler loop + negative pion handler loop with the condition that both pions come from the same event.
- Neutral and positive pions from the same event: negative pion candidates from same event as the neutral pion loop + positive pion handler loop.
- Neutral and negative pions from the same event: positive pion candidates from same event as the neutral pion loop + negative pion handler loop.

The different correlation cases will produce different background description results, plotted below. The histograms will be two-dimensional, associating the invariant mass with the p_t.

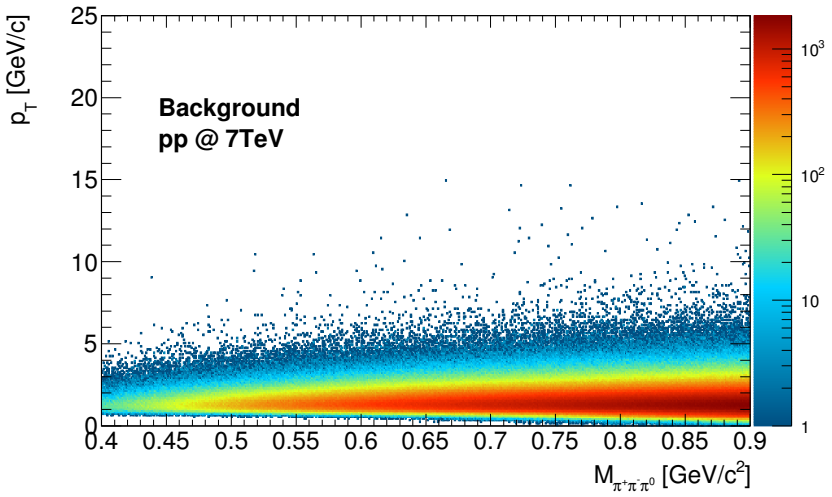

Figure 19: Background Group 1- Charged pions from the same event

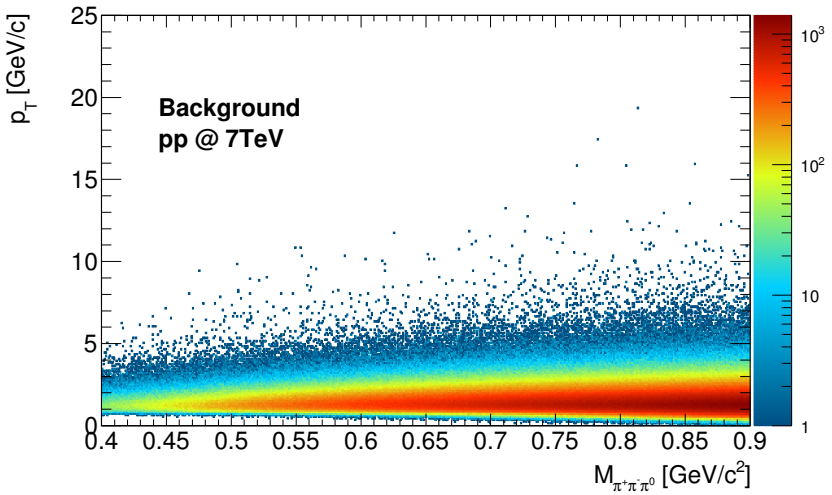

Figure 20: Background Group 2 - Neutral and positive pions from the same event

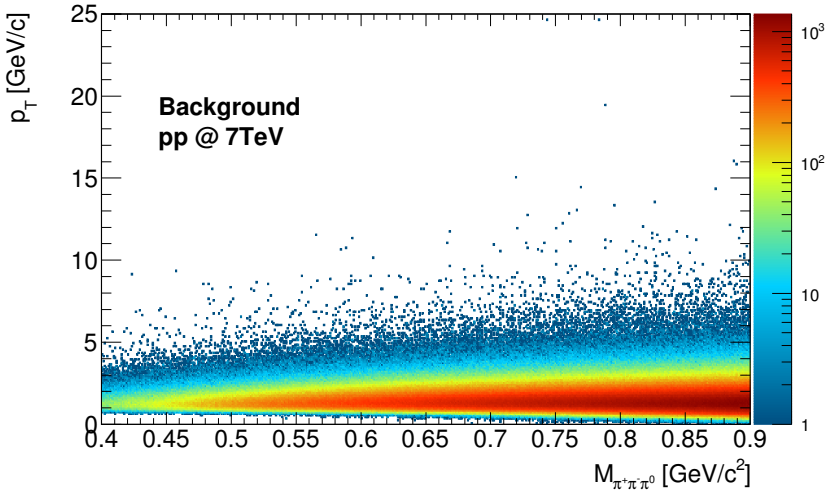

Figure 21: Background Group 3 - Neutral and negative pions from the same event

One can observe that the three backgrounds are differently described. Taking this into account, the total invariant mass background will be a combination of all three cases. This combination will be simply a sum of them:

$$B_t = aB_1 + aB_2 + aB_3 \tag{12}$$

In this equation, B_t is the total background. The parameter a is equal for the three cases, once the weighting is equal: B_1, B_2 and B_3 contributions are the same.

The background needs to be normalized after this sum procedure, once the number of the background plot entries is bigger than the $M_{\pi^+\pi^-\pi^0}$ number of entries. This happens due to all possible event combinations inserted in the background histogram. This normalization can be made in different ways, but all of them use the same the formula for the normalization factor F_n calculation:

$$F_n = \frac{\text{Signal + Background Area}_{|\text{selected mass range}}}{\text{Background Area}_{|\text{selected mass range}}} \tag{13}$$

The different ways to normalize the background, as cited before, depend on the determined mass range. The selected mass range to calculate the area will be located at the right or at the left side of the peak. Another possibility is to calculate the two different areas (left and right) simultaneously. When the normalization factor is finally calculated, the whole background is scaled to the signal + background histogram with this factor.

It's important to remark that the left side area can't be calculated within the eta particle peak interval, or the background description won't be good. In this task, the left mass range is chosen to be between 0.615 GeV/c^2 and 0.69 GeV/c^2 and the right mass range to be between 0.82 GeV/c^2 and 0.89 GeV/c^2.

The histogram below illustrates the three background types for the right normalization case:

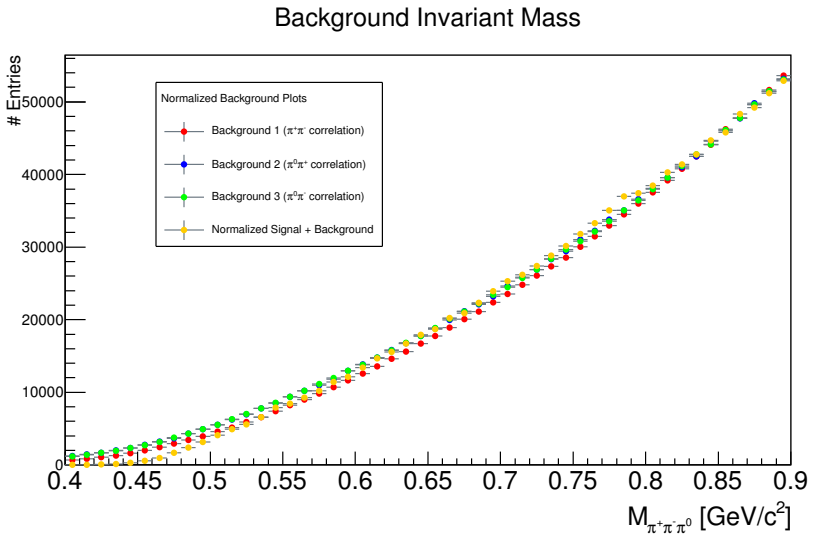

Figure 22: Three different background possibilities drawn with signal

The omega peak is visible in the background + signal curve.

After this step, the background can be subtracted and the signal takes the form of a gaussian peak. This is fitted to find the obtained omega mass with the number of sigmas of this gaussian being the uncertainty. The fit is a sum of a gaussian and a exponential to represent the Bremsstrahlung on the left side of the peak and a linear to represent the resultant background.

6 Results

This section will present the background and omega peak results for data and Monte Carlo, for the simultaneous left+right and for the right normalization. The omega raw yield for data and the corrected yield are also presented, the last one based on geometrical acceptance and reconstruction efficiency calculations.

6.1 Data Results

The first result below (Figure 23) shows the encountered background for different transverse momentum intervals, plotted together with the invariant mass histograms. In this scheme, it's possible to see that the PCM reproduces a big amount of entries in the invariant mass histogram when the transverse momentum is low/intermediate. Also visible is the difficulty to describe the background in a high p_t interval, due to the small number of events in this region.

The figure 24 shows the diverse omega peaks after the background subtraction, for the same p_t bins presented in figure 23. The peak form changes with the time. The larger the data amount, the smaller the uncertainty, because the only associated errors come from statistics.

Similar observations can be made for figures 25 and 26. The only differences between them are the parameters used for the normalization: in the figures 23 and 24, the normalization factor is calculated for two mass ranges simultaneously, to the left and to the right side of the peak. In the next figures, the used mass range to calculate the areas for normalization is located at the right side of the peak.

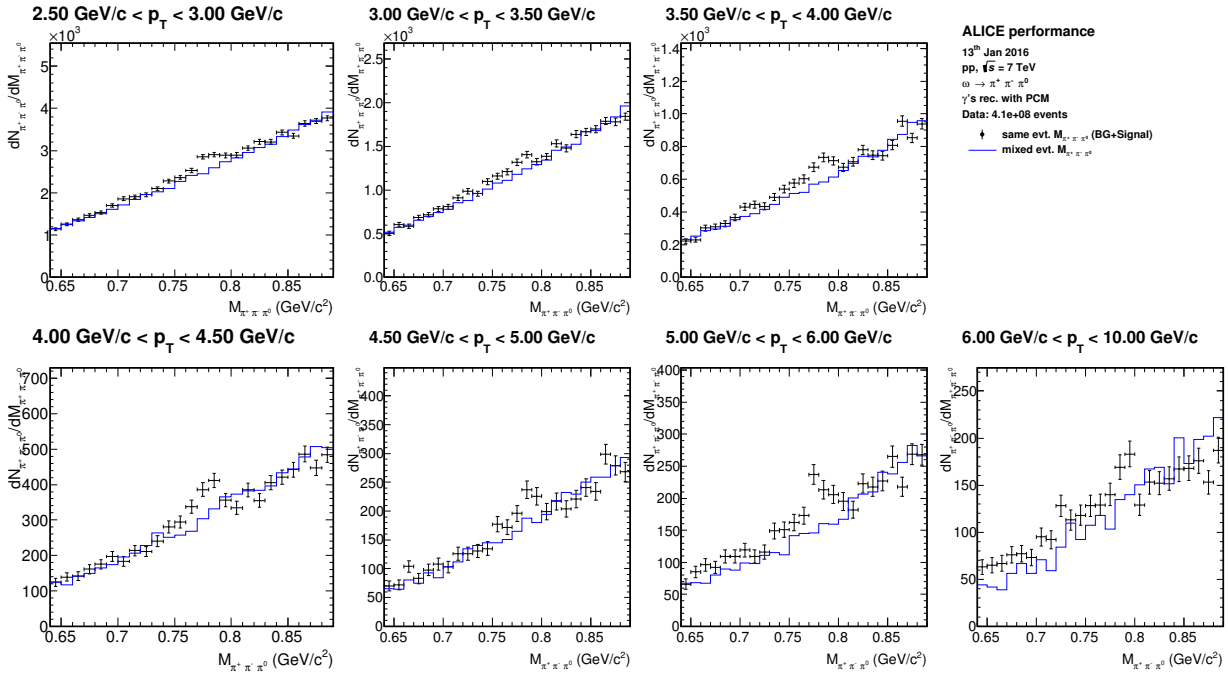

Figure 23: Background description with left-right normalization factor - data

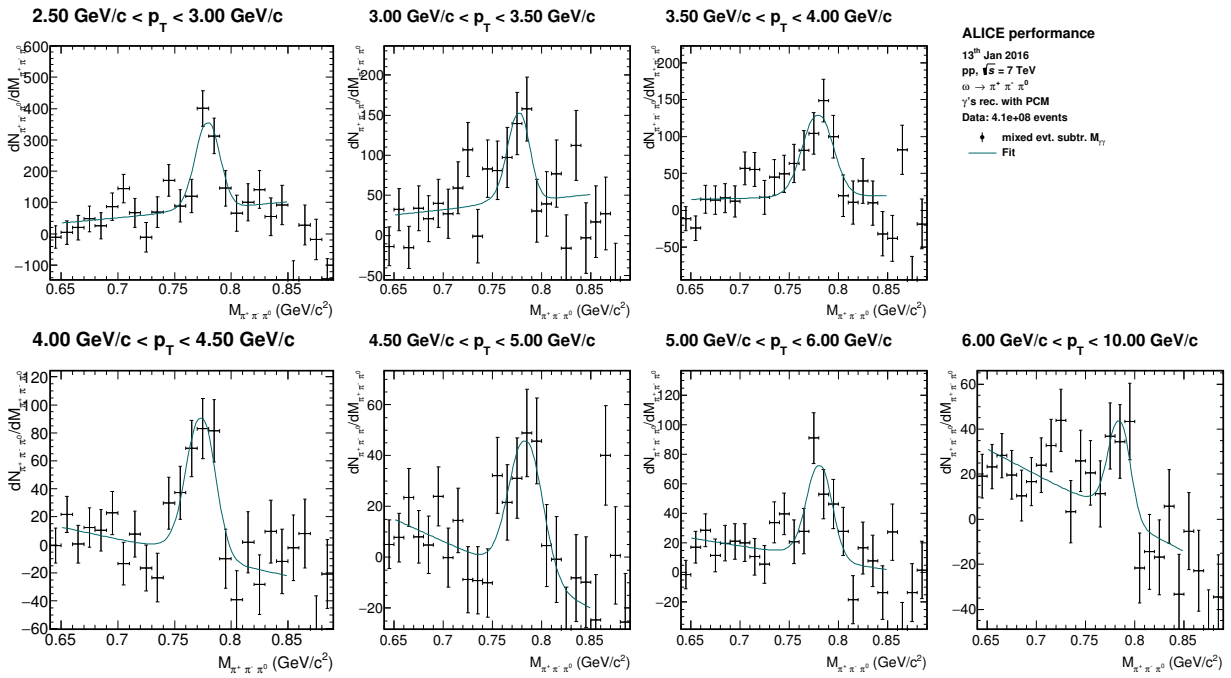

Figure 24: Subtracted background with left-right normalization factor - data

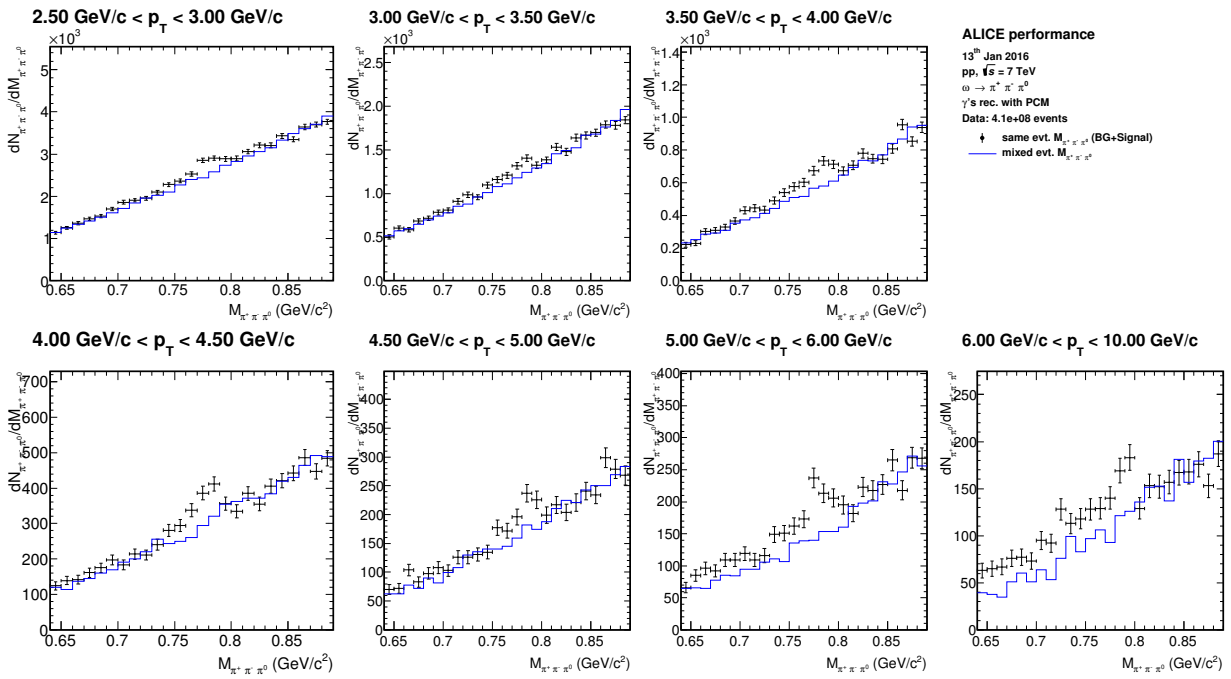

Figure 25: Background description with right normalization factor - data

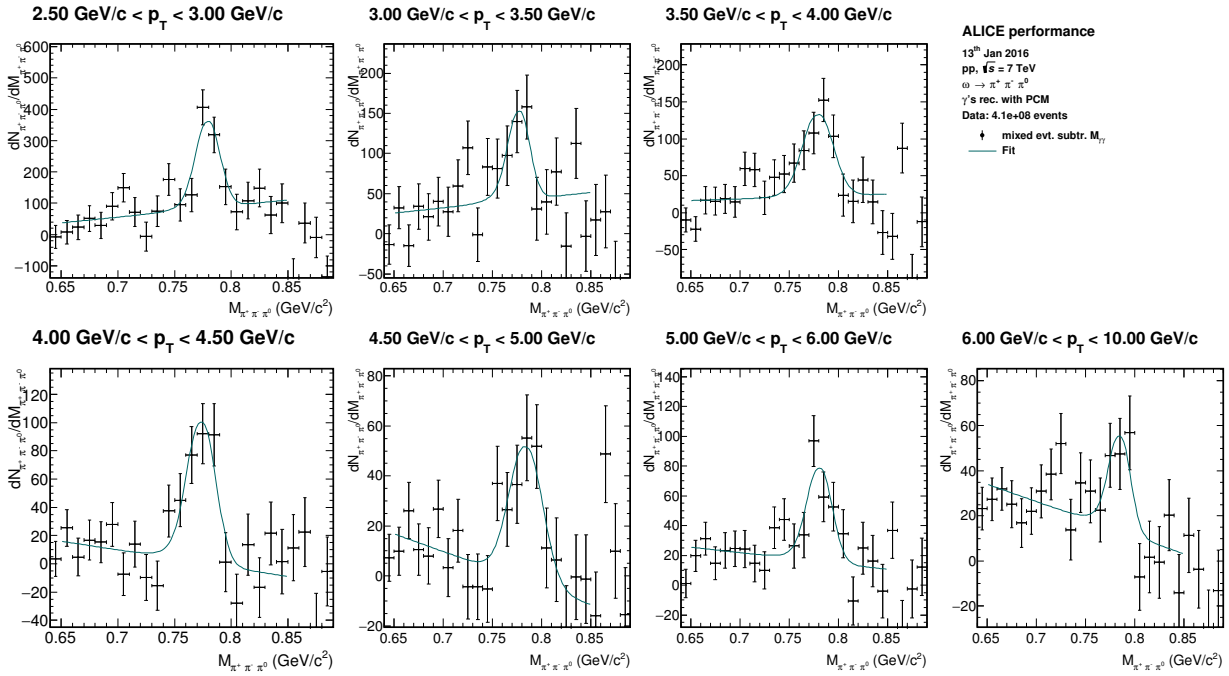

Figure 26: Subtracted background with right normalization factor - data

Raw yields are calculated with the integral of the encountered peaks. These integrals are calculated with three different configurations, which can determine the omega peak integral ranges to be narrow, wide or with standard parameters. In this case, the presented results will always be calculated with standard parameters. The standard integration range for this analysis is between 0.74 GeV/c^2 and 0.83 GeV/c^2.

The presented result illustrate the omega meson yield, without any correction. The corrections are performed only when MC plots are generated, because they can ask for true omegas, and calculate the detector real acceptance and reconstruction efficiency.

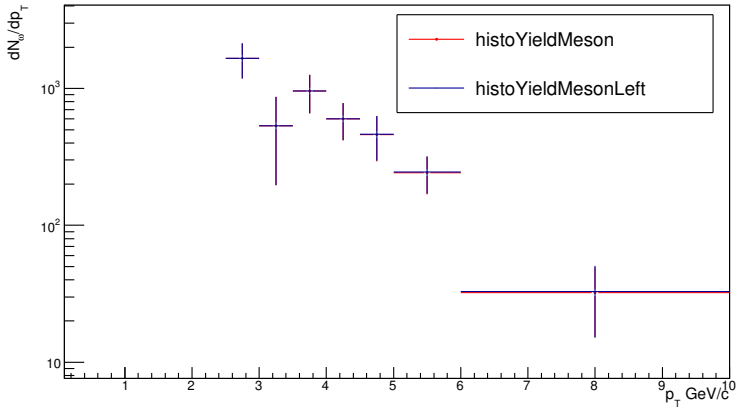

Figure 27: Omega raw yield - data

In the legend, histoYieldMeson is calculated with the standard right normalization and histoYield-MesonLeft with the left-right normalization.

6.2 Monte Carlo Results

The MC signal extraction is performed and the true omegas are then called [43]. Observing the produced histograms, similar conclusions to the ones found in data can be made. But in the MC context, some additional observations can be done: in the figures 29 and 31, for all p_t bins, the fitting function is a little bit above the true omegas curve, whereas the background shouldn't be present anymore. Some plots, like for 4.0 GeV/c $< p_t <$ 4.5 GeV/c and for 4.5 GeV/c $< p_t <$ 5.0 GeV/c, have the encountered omega peak wider than the true peak. This represents probably a small error in the applied integration ranges.

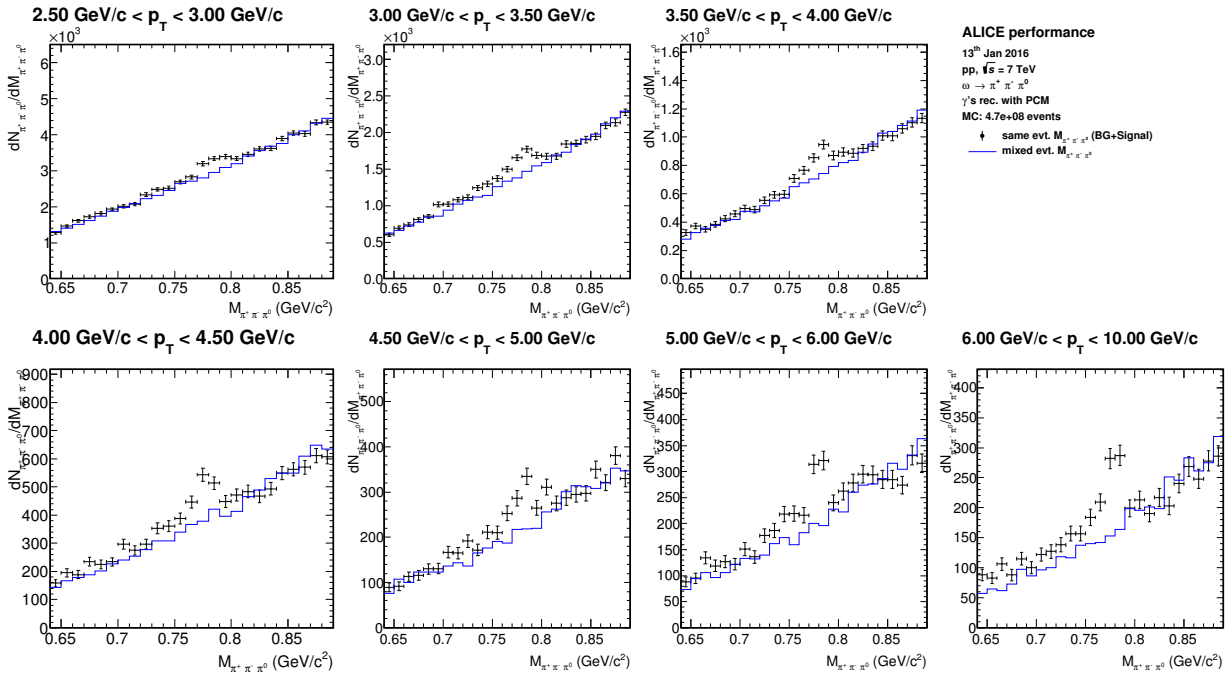

Figure 28: Background description with left-right normalization factor - Monte Carlo

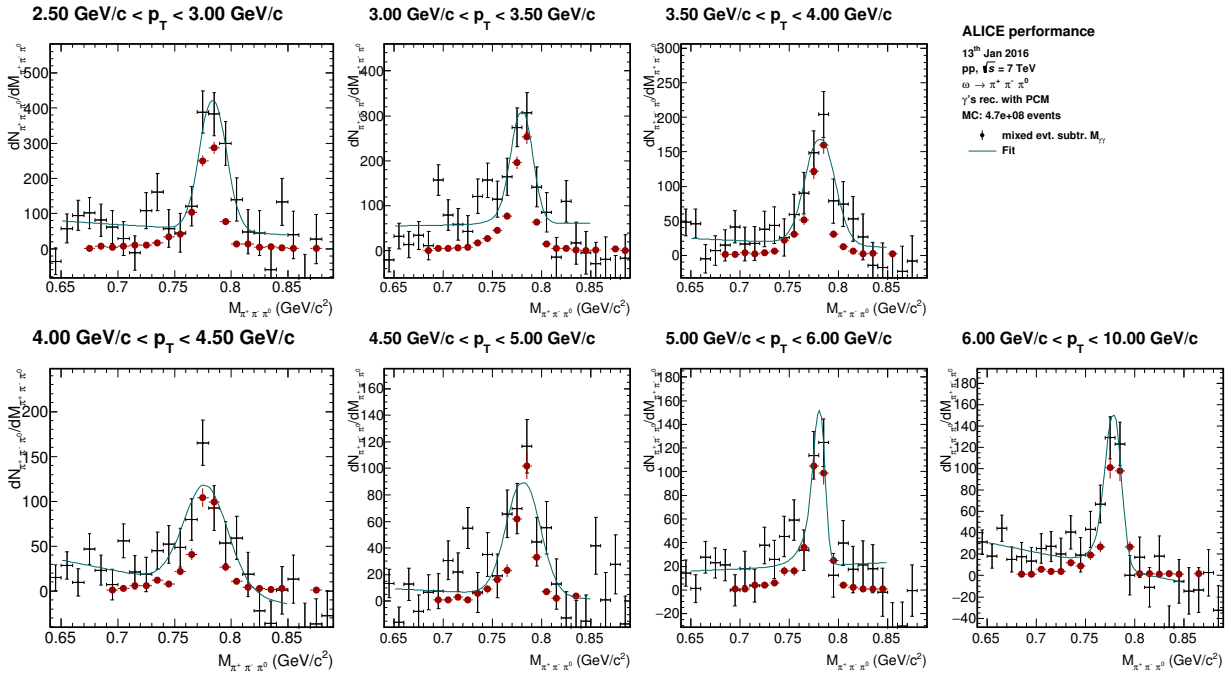

Figure 29: Subtracted background with left-right normalization factor - Monte Carlo

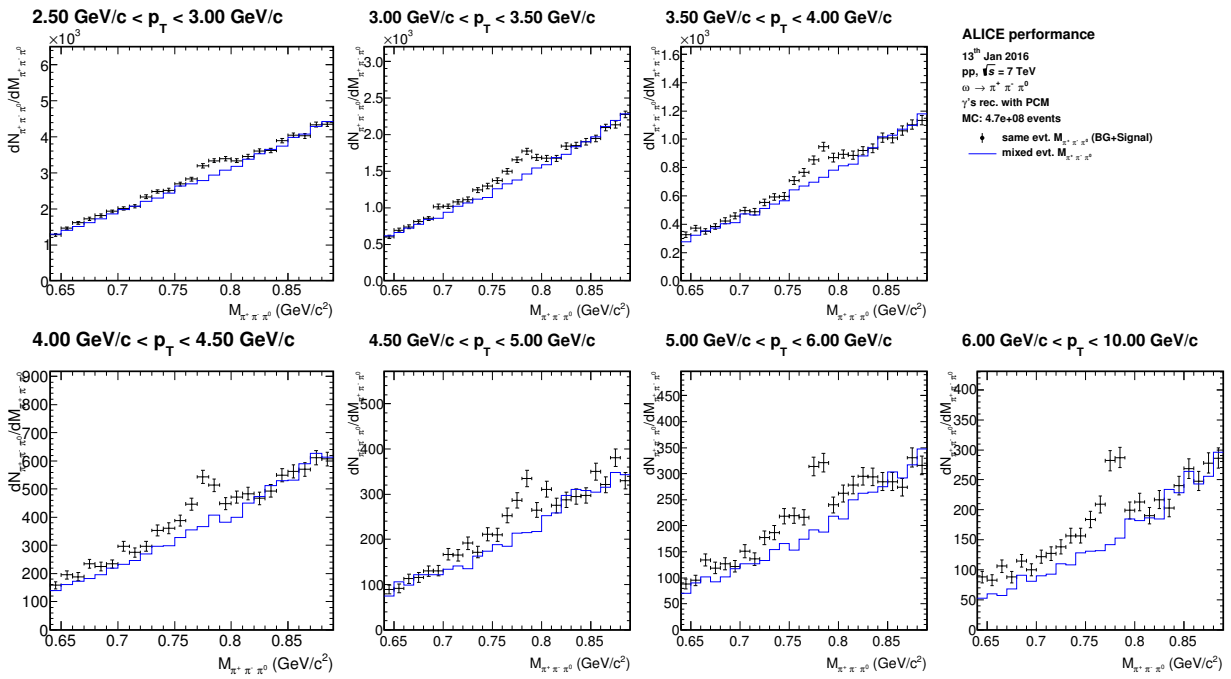

Figure 30: Background description with right normalization factor - Monte Carlo

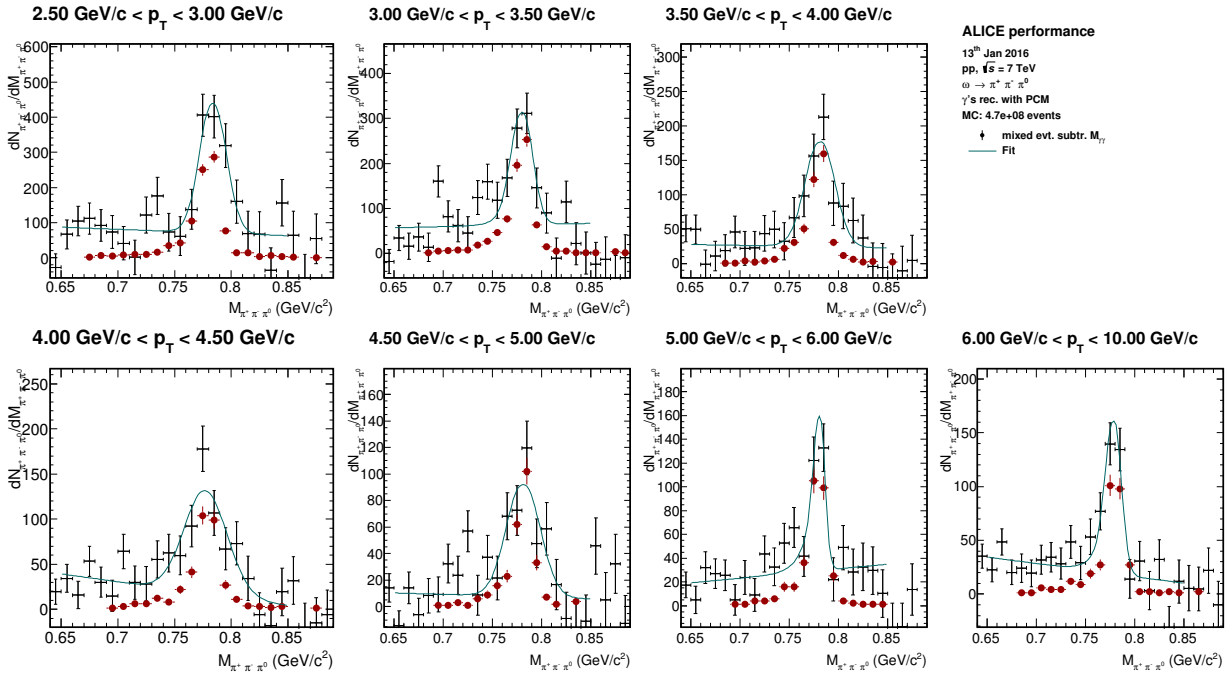

Figure 31: Subtracted background with right normalization factor - Monte Carlo

Once the MC simulations are done, the meson reconstruction efficiency and the detector geometrical acceptance calculations become possible. For the efficiency calculation, MC data is handled as real data. The difference between it and the true produced omegas will correspond to the reconstruction efficiency [43].

The geometrical acceptance Acc_ω is on the other hand calculated using the formula [43]:

$$Acc_\omega = \frac{N_{\omega,|y|<0.8} \text{ with the daughter particles within } |\eta_{\pi^0}| < 0.9, |\eta_{\pi^\pm}| < 1.4}{N_{\omega,|y|<0.8}} \tag{14}$$

In this formula, $N_{\omega,|y|<0.8}$ represents the omega raw yield within the given rapidity range and daughter particles pseudorapidity range. Plots with the calculated acceptance and efficiency are illustrated below:

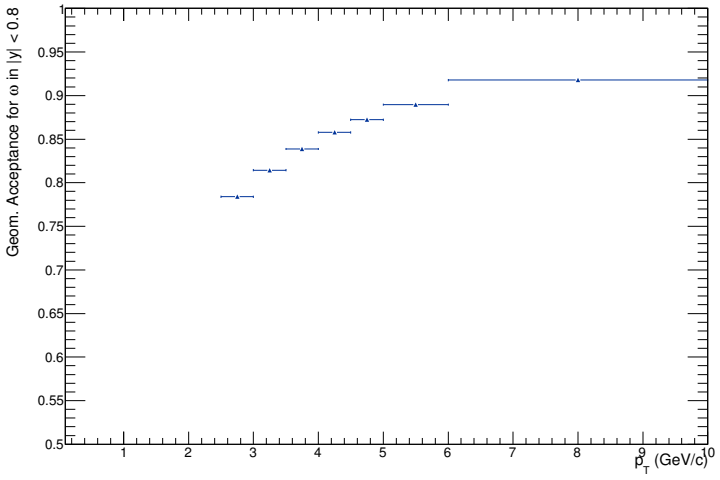

Figure 32: Geometrical acceptance factor - Monte Carlo

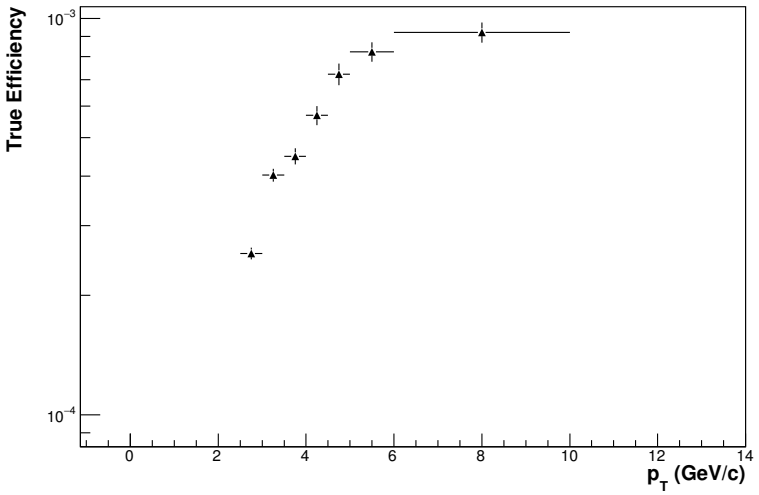

Figure 33: Reconstruction efficiency factor - Monte Carlo

Oberving the plots, it is possible to see that the acceptance increases slowly with an increasing transverse momentum.

The efficiency decreases sharply with a decreasing p_t. In this histogram, it is possible to see that the reconstruction efficiency is very low. This happens mainly because the probability of a photon to produce an e^-e^+ pair is low (approximately 8.5%) and the pure PCM considers two gamma conversions, i.e. 8.5% x 8.5%. The track efficiency also depends on the V0 finder and tracking efficiencies and on the probability of pions and omegas to decay.

6.3 Yield Correction

The yield correction is calculated using the formula:

$$Correction = \frac{1}{2\pi N_{events}} \frac{1}{p_T} \frac{1}{BR} \frac{1}{Acc_{(w)}\epsilon_\omega} \frac{N_\omega}{\Delta y \Delta p_T} \tag{15}$$

In this equation, (N_{events}) represents the number of Minimum Bias events and N_ω the omega raw yield, which will be divided for the rapidity range Δy and for Δp_T, the transverse momentum at the bin center [44]. The other parameters are already known.

Results from the correction, when applied to the data, will give the final plots to analyse:

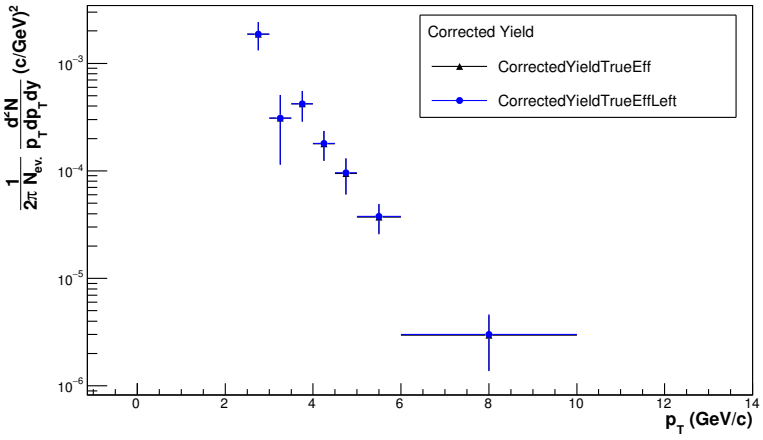

Figure 34: Meson corrected Yield

In the legend, CorrectedYieldTrueEff is the corrected yield with the standard right normalization, and CorrectedYieldTrueEffLeft with the left-right normalization.

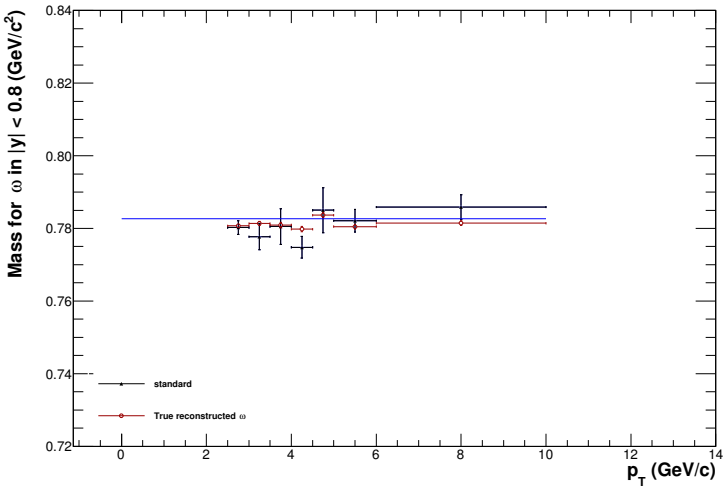

Figure 35: Omega Mass in Comparison to the PDG - Monte Carlo

The first histogram shows the meson corrected yield. It is possible to observe that the omega yield decreases with an increasing p_t, as expected. The second point or the four next ones could be deviated,

since they don't follow a tendence line. The omega mass plot is although compatible with the PDG data, represented by the blue line.

6.4 ω/π^0 Ratio

The figure below shows the ω/π^0 ratio result. Although a constant fit was made, another fit could also be possible. The result does not show, however, conclusive points. The constant fit parameter was found automatically and the encountered parameter representing the ratio is 1.12 with a χ^2 of 4.37 and a p-value of 49.74%.

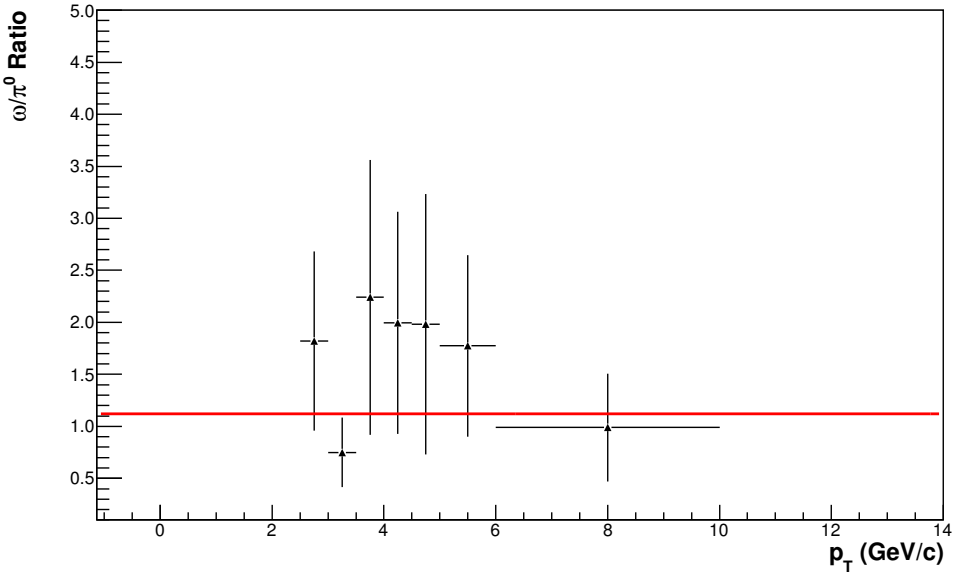

Figure 36: The ω/π^0 ratio

7 Conclusions and Outlook

From the plots, one can observe that the peaks were reasonable fitted, although there's a little background left. This fact can happen because of background fluctuations or errors during the normalization, such as not appropriated range parameters. One possible consideration to make is that the normalization ranges need to be different for each p_t interval, since the peaks have different forms for each transverse momentum range. The second or the four next points from the corrected yield have a certain deviation from what would be a tendence line. The error for the ω/π^0 ratio could also be somehow wrong calculated, since it shouldn't be so big.

Some issues need to be considered for the outlook:

- The used task needs to be adapted for the cases in which the photons are reconstructed with pure calorimeter and with calorimeter-PCM reconstruction methods,
- The analysis needs to be tested for another center-of-mass energies,
- Normalization ranges need to be aprimorated for the different integral calculations,
- The used task needs to be tested for the eta particle, since it also decays in the same three pions,
- The cuts can be optimized,
- A refined analysis needs to be made, for the systematic errors calculation.

8 Acknowledgements

I wanted to say that I'm very grateful to all the people who collaborated with me and supported me during the time I was doing this work. That's why I want to give an especial thanks to

- Prof. Johannes Wessels and Priv. Doz. Dr. Christian Klein-Bösing, due to the given opportunity,
- Denise Godoy and Daniel Mühlheim, for all the help and patience,
- My mother Eliane, my father Marcio, my brother Renan and my grandparents. They were always comprehensive and told me since I was a kid that I needed to go after all things that interested me,
- My boyfriend Luan, who always understood my ambitions,
- The people in the Kernphysik-Institut from the University of Münster, who received me so well,
- My friends Juliana, Verônica, Dafne, Federica and Zozan, for the incredible company during my stay in Germany,
- My professors in the university in Brazil (Universidade Federal de São Carlos),
- My teachers Marcelo Barão and Gilmar Mignaco from my school in Brazil. They were the ones who encouraged me the most, who taught me not only equations, but values that I'm going to use for a lifetime.

References

[1] MOREIRA, Marco Antonio. O Modelo Padrão da Física de Partículas. Rev. Bras. Ensino Fís., São Paulo , v. 31, n. 1, p. 1306.1-1306.11, Apr. 2009 .

[2] URL: http://cms.web.cern.ch/news/what-do-we-already-know .

[3] HARRIS, John W.; MLLER, Berndt. The search for the quark-gluon plasma. arXiv preprint hep-ph/9602235, 1996.

[4] FERREIRA, Luellerson Carlos; MOTA, André Luiz. A Anomalia Quiral no Modelo de Quarks Espectral.

[5] SATZ, Helmut. The transition from hadron matter to quark-gluon plasma. Annual Review of Nuclear and Particle Science, v. 35, n. 1, p. 245-270, 1985.

[6] ALFORD, Mark. Viewpoint: Cool quarks. Physics, v. 3, p. 44, 2010. Illustration by Alan Stonebraker.

[7] STEPHANOV, Mikhail A. QCD phase diagram and the critical point. Prog. Theor. Phys., Suppl., v. 153, n. hep-ph/0402115, p. 139-156, 2004.

[8] SCHMIDT, N. Neutral Pion Measurements with Conversions in ALICE in pp Collisions at $\sqrt{(s)}$ = 8 TeV. Bachelor Thesis, University of Heidelberg, 2014.

[9] K.A. Olive et al (Particle Data Group). Review of Particle Physics. Chin.Phys.C38 (2014), p. 090001. doi: 10.1088/1674-1137/38/9/090001.

[10] KOCH, Alexander. Eta meson production with conversions in ALICE in pp collisions at $\sqrt{s}$ = 2.76 TeV and $\sqrt{s}$ = 8 TeV. Bachelor Thesis. University of Heidelberg.

[11] URL: http://ocw.mit.edu/courses/nuclear-engineering/22-01-introduction-to-ionizing-radiation-fall-2006/lecture-notes/energy_dep_photo.pdf .

[12] BOCK, F. ALICE Capabilities for Studying Photon Physics with the Conversion Method at LHC Energies. Bachelor Thesis, University of Heidelberg, 2010.

[13] YOSHIMURA, Elisabeth Mateus. Física das Radiações: interação da radiação com a matéria. Revista Brasileira de Física Médica, v. 3, n. 1, p. 57-67, 2009.

[14] TOLOS, Laura et al. The width of the ω meson in dense matter. arXiv preprint arXiv:1401.1991, 2014.

[15] GODFREY, Stephen; ISGUR, Nathan. Mesons in a relativized quark model with chromodynamics. Physical Review D, v. 32, n. 1, p. 189, 1985.

[16] NICHITIU, F. An Introduction to the Vector Meson. 1995.

[17] K.A. Olive et al. (Particle Data Group), Chin. Phys. C38 , 090001 (2014) (URL: http://pdg.lbl.gov).

[18] URL: http://www.hep.shef.ac.uk/edaw/PHY206/Site/2012$_course_files/phy206rlec7.pdf$

[19] RANDALL, Lisa. Knocking on Heaven's Door: How Physics and Scientific Thinking Illuminate the Universe and the Modern World. Random House, 2011.

[20] NÓBREGA, Fábio Kopp; MACKEDANZ, Luiz Fernando. The LHC (Large Hadron Collider) and our daily physics. Revista Brasileira de Ensino de Física, v. 35, n. 1, p. 1-11, 2013.

[21] URL: http://home.cern/about/experiments/atlas .

[22] URL: http://home.cern/about/experiments/cms .

[23] URL: http://home.cern/about/experiments/alice .

[24] URL: http://home.cern/about/experiments/lhcb .

[25] HAFFNER, Julie. The CERN accelerator complex. 2013.

[26] CARMINATI, F. et al. ALICE: Physics performance report, volume I. Journal of Physics G: Nuclear and Particle Physics, v. 30, n. 11, p. 1517, 2004.

[27] COLLABORATION, ALICE et al. The ALICE experiment at the CERN LHC. Jinst, v. 3, n. 420, p. S08002, 2008.

[28] URL: http://alice-collaboration.web.cern.ch/ .

[29] BOCK, F. Neutral Pion and Eta Meson Production in pp and Pb-Pb Collisions at the LHC with the ALICE Detector. 2012. Master thesis, University of Heidelberg.

[30] URL: http://alipub.web.cern.ch/detectors/more-details-alice-tpc .

[31] URL: http://alipub-dev.web.cern.ch/detectors/more-details-emcal .

[32] CORTESE, P. et al. ALICE technical design report on forward detectors: FMD, T0 and V0. 2005.

[33] ALICE COLLABORATION et al. Performance of the ALICE VZERO system. arXiv preprint arXiv:1306.3130, 2013.

[34] DE GODOY, Denise Aparecida Moreira. Anisotropia azimutal elptica de eltrons de decaimentos de quarks pesados em colises de Pb-Pb. 2013. Tese de Doutorado. Universidade de So Paulo.

[35] KOCH, Kathrin. Measurement of π^0 and η mesons with photon conversions in ALICE in proton-proton collisions at $\sqrt{(s)} = 0.9$, 2.76 and 7 TeV. 2012.

[36] K.A. Olive et al.(Particle Data Group), Chin. Phys. C, 38, 090001 (2014) and 2015 update

[37] ALICE COLLABORATION et al. Performance of the ALICE Experiment at the CERN LHC. arXiv preprint arXiv:1402.4476, 2014.

[38] URL: https://twiki.cern.ch/ .

[39] BALBASTRE, G. C. et al. π^0 identification with EMCAL via shower shape and cluster splitting analysis methods in ALICE. ALICE-ANALYSIS-NOTEANA145, 2012.

[40] SJÖSTRAND, Torbjörn; MRENNAC, Stephen; SKANDSA, Peter. A Brief Introduction to PYTHIA 8.1. arXiv preprint arXiv:0710.3820, 2007.

[41] SJÖSTRAND, Torbjörn. PYTHIA 8 status report. arXiv preprint arXiv:0809.0303, 2008.

[42] BAUMEIER, David. V0 Decays: Documentation of the C++ Program AliESDv0KineCuts.cxx. Bachelor Thesis. University of Mnster.

[43] BICIAN, Lubos. Reconstruction of neutral mesons using photon conversions. 2014.

[44] ABELEV, Betty et al. Neutral pion and η meson production in protonproton collisions at $sqrts = 7$TeV . Physics Letters B, v. 717, n. 1, p. 162-172, 2012.